MNRAS 000, 1–21 (2025) Preprint 28 October 2025 Compiled using MNRAS LaTeX style file v3.3

Photometric and Spectroscopic Studies of Four Low Mass-ratio Contact Binaries with Period Longer than 0.7 days

Yi-Fan Wang,[1] Kai Li,[1★] Fei Liu,[1] Xin Xu,[1] Mu-Zi-Mei Li,[1] Cheng-Yu Wu,[1] Yu-Tong Li,[2†] Yan-Ke Tang,[2] Xing Gao[3] and Guo-You Sun[4]

[1]*Shandong Key Laboratory of Space Environment and Exploration Technology, Institute of Space Sciences, School of Space Science and Technology, Shandong University, Shandong, China*

[2]*Shandong Key Laboratory of Space Environment and Exploration Technology, College of Physics and Electronic information, Dezhou University, 566 West University Road, Decheng District, Dezhou 253023, China*

[3]*Xinjiang Astronomical Observatory, 150 Science 1-Street, Urumqi 830011, People's Republic of China*

[4]*Xingming Observatory, Urumqi 830002, Xinjiang, People's Republic of China*

Accepted XXX. Received YYY; in original form ZZZ

ABSTRACT

Photometric and spectroscopic studies of four long-period low mass-ratio contact binaries, V0508 And, V0844 Aur, V0699 Cep, and NSVS 6259046, are performed. V0508 And, V0844 Aur, and V0699 Cep are found to be A-type low-mass-ratio medium-contact binaries, while NSVS 6259046 is found to be an A-type deep-contact binary. $O-C$ analysis indicates no long-term variation in V0844 Aur. However, the orbital periods of the other three targets are increasing. We conclude that V0844 Aur, V0699 Cep and NSVS 6259046 are magnetically active, as evidenced by the presence and variable nature of the O'Connell effect in these systems. By analyzing the LAMOST spectroscopic data, we find out that NSVS 6259046 and V0508 And exhibit no chromospheric activity on the dates the LAMOST spectra were taken, while the low signal-to-noise ratio in LAMOST data for V0844 Aur prevents us from obtaining reliable results. We discover that V0699 Cep is an early-type contact binary with chromospheric activity. Their initial masses and ages are calculated. All four systems are determined to be currently stable. We collect 217 contact binaries with both spectroscopic and photometric observations, and compare the differences between short-period and long-period systems in terms of mass–luminosity relation and mass–radius relation, using 0.7 days as the period boundary.

Key words: binaries (including multiple): close – binaries: eclipsing – stars: evolution – stars: individual.

1 INTRODUCTION

Contact binaries serve as fundamental astrophysical laboratories for exploring stellar structure, formation mechanisms, and evolutionary pathways (Qian 2003; Yakut & Eggleton 2005; Li et al. 2007; Eker et al. 2008a; Eggleton 2012; Poro et al. 2024a). Numerous unresolved questions still exist after decades, including the orbital period cutoff (Li et al. 2019b; Zhang et al. 2023), mass ratio limit (Williams & Roxburgh 1976; Rasio 1995; Arbutina 2007, 2009; Li et al. 2022a, 2024), and the O'Connell effect (O'Connell 1951), all of which require more investigation.

In the galactic disk, one in every 500 F,G,K-type main-sequence stars is considered to be a contact binary (CB) (Rucinski 2006). CBs are systems consisting of two components covered by a common convective envelope (Lucy 1968), meaning that their surface temperatures are the same. The early known samples of CBs exhibited two key limitations: their numbers were substantially smaller, and due to the lower photometric precision at that time, the samples were biased toward systems with higher inclination angles. As clearly demonstrated in Figure 2 of Kobulnicky et al. (2022), in such high-inclination configurations, the primary minimum is roughly equal to the second minimum (Kuiper 1941; Kraft 1967; Lucy 1967b, 1968). Due to the common convective envelope, there is energy and mass transfer between the two components, leading to changes in orbital period (e.g. Li et al. 2015b; Liao et al. 2017; Lee & Park 2018; Li et al. 2019a), and theories of thermal relaxation oscillations (e.g. Flannery 1976; Lucy 1976; Robertson & Eggleton 1977). CBs are classified into two types (Binnendijk 1970): type A and type W. For type A, the surface temperature of the more massive star is higher than that of the less massive star. Conversely, type W corresponds to the opposite situation compared to type A.

Magnetic activities in contact binaries include star spots, flares, and plages (Pribulla et al. 2003b). These phenomena are closely related to convective motions and rapid stellar rotation (Strassmeier 2009). Magnetic activity may cause noticeable asymmetry in the light curve maxima, a phenomenon known as the O'Connell effect (O'Connell 1951). It is attributed to mechanisms such as cool spots due to magnetic activity (Li et al. 2016b), mass accretion (Shaw 1994; Park et al. 2013), circumstellar material (Liu & Yang 2003), and asymmetry of circumfluence from the Coriolis effect (Zhou & Leung 1990). Magnetic activities can influence the orbital period of CBs

★ E-mail: kaili@sdu.edu.cn
† E-mail: qiuwutongyu622@163.com

noticeable (Applegate 1992). As for spectroscopic analysis, there are special emission lines indicating chromospheric activity, such as Ca II H&K, Balmer series, and Ca II triplet above the continuum (Pavlenko et al. 2018; Cheng et al. 2019; Long et al. 2019; Zheng et al. 2021). Spectroscopic emission lines such as H_α provide direct evidence of intense magnetic activities on the stellar surface, often in conjunction with rapid rotation (Wilson 1978).

The study of mass ratio and orbital period is important for understanding the evolution of CB. Molnar et al. (2019, 2022) developed angular momentum conserving models to explain the evolution of CBs, showing a relationship between orbital period and the lower limit of the mass ratio. Based on the models above, Kobulnicky et al. (2022) analyzed the relationship of mass ratios and orbital periods in CBs. They found that the critical instability mass ratio increases from 0.045 to 0.15 as the orbital period grows from 0.74 to 2.0 days. However, research on CBs with orbital periods longer than 0.7 days are currently rare (Molnar et al. 2019, 2022; Liu et al. 2024; Li et al. 2025). While the evolutionary processes of all CBs still present numerous unresolved questions, the evolutionary pathways of long-period systems are particularly poorly understood. Further research on long-period low mass-ratio CBs is necessary.

To study long-period low mass-ratio CBs, we select four totally eclipsing CBs based on specific criteria: orbital periods > 0.7 days and amplitudes < 0.4 mag. The amplitude criterion is motivated by Rucinski (2001), who established a correlation between amplitude and mass ratio, implying that small-amplitude systems are likely to have low mass ratios. Guided by this relationship, we identify four candidate systems from the All Sky Automated Survey for SuperNovae (ASAS-SN) (Shappee et al. 2014; Kochanek et al. 2017; Jayasinghe et al. 2019). The fundamental parameters of the selected CBs are summarized in Table 1.

2 OBSERVATIONS

2.1 Photometry

The photometric observations of four binary star systems are conducted using the Ningbo Bureau of Education Telescope and the Xinjiang Observatory Telescope (NEXT) at the Xingming Observatory. The NEXT features a 60 cm aperture telescope and is equipped with an FLI PL23042 back-illuminated CCD camera that has a 2048 × 2048 pixel array, providing a field of view of approximately 22′ × 22′. All raw images are processed for bias, dark, and flat corrections using C-MuniPack software designed for photometric data processing. Aperture and differential photometry methods are employed for data analysis. Details of our observation are presented in Table 2. Subsequently, differential magnitudes are calculated between the target object and the comparision star, as well as between the comparision star and the check star. The photometric data are presented in Table 3, where Δm represents the instrumental magnitude difference between the variable star and the comparison star. All four targets are total-eclipse CBs, with total eclipses lasting 0.123 of an orbit for V0508 And, 0.058 for V0844 Aur, 0.039 for V0699 Cep and 0.148 for NSVS 6259046.

To get a longer time baseline for $O-C$ analysis, we proceed to leverage the archival photometry. Our four systems have also been observed by various photometric surveys, including the Transiting Exoplanet Survey Satellite (TESS) (Ricker et al. 2015), the All-Sky Automated Survey for Supernovae (ASAS-SN) (Shappee et al. 2014; Jayasinghe et al. 2019), the Super Wide Angle Search for Planets (SuperWASP) (Butters et al. 2010), and the Zwicky Transient Facility (ZTF) (Bellm et al. 2019; Masci et al. 2019).

2.2 Spectroscopy

The Large Sky Area Multi-Object Fiber Spectroscopic Telescope (LAMOST), which possesses a 4-meter aperture and is a unique reflecting Schmidt telescope with a 5° field of view, collects numerous stellar spectra (Cui et al. 2012; Zhao et al. 2012). The resolution in low-resolution mode is approximately 1800 (Wang et al. 1996), with wavelength ranging from 3700 to 9000 Å (Du et al. 2016). The telescope incorporates 4000 fibers on its surface, significantly enhancing the speed of spectrum collection (Cui et al. 2012). LAMOST records all of our targets in low resolution. We download the data in DR11. The spectral parameters of the four targets are demonstrated in Table 4.

3 PHOTOMETRIC SOLUTION

Photometric analysis involves the use of the Wilson-Devinney (W-D) software (Wilson & Devinney 1971; Wilson 1979, 1994), version 2013, for solving the light curves. We use LAMOST $T_{\rm eff}$ as the effective temperature of each target initially, which is fixed during the W-D procedure. However, for V0844 Aur, due to the low signal-to-noise ratio, the effective temperature is given by its F5 spectral type, which is 6550 K, according to the Table 5 of Pecaut & Mamajek (2013). All $T_{\rm eff}$ of our four targets are below 7200 K. When $T_{\rm eff}$ < 7200 K, gravitational darkening is assumed to be $g = 0.32$ (Lucy 1967a), and bolometric albedo coefficient is set at $A = 0.5$ for both components (Ruciński 1969). Using square root law, we interpolate Van Hamme (1993)'s table to obtain the limb-darkening coefficients. The parameter q is computed using q-search method. Adjustable parameters include orbital inclination i, effective temperature of the less massive star T_2, luminosity of the massive star L_1, and potential ($\Omega_1 = \Omega_2 = \Omega$). To check whether our four targets exhibit third light, we also consult the Gaia [1] database and find that only V0699 Cep shows evidence of third light within our photometric aperture. Table 5 presents data for objects within a 5-magnitude range of our targets based on Gaia DR3, mean g-band photometric flux of V0699 Cep is 348708.7 electron $\cdot$ s^{-1} , and the third light's is 100942.6 electron $\cdot$ s^{-1}, we calculate that the flux contribution of the third light is 22.4%, therefore third light is also chosen as a free parameter for V0699 Cep. This method only weeds out certain kinds of tertiaries, such as more massive companions at large enough separations to produce astrometric deviations. It does not rule out the presence of tertiary stars in relatively small orbits. The relationship between q and the mean residual is shown in Fig. 1. q with minimum mean residuals is obtained, then we set it as the initial value and an adjustable parameter to obtain a convergent solution. As $T_{\rm eff}$ represents the integrated temperature of both primary and secondary components, we use the following equations to calculate the temperatures of both the primary and secondary stars (Zwitter et al. 2003),

$$T_1 = \left(\frac{\left(1 + \left(\frac{r_2}{r_1}\right)^2\right) T_{\rm eff}^4}{1 + \left(\frac{r_2}{r_1}\right)^2 \left(\frac{T_2}{T_1}\right)^4} \right)^{0.25}, \quad (1)$$

$$T_2 = T_1 \times \frac{T_2}{T_1}, \quad (2)$$

We set more accurate temperatures as initial values in W-D program, while the primary temperature is fixed and the secondary temperature

[1] https://gea.esac.esa.int/archive/

Table 1. The ASAS-SN name, period, mean V-band magnitude and color indices of the four investigated targets.

Targets	ASAS-SN name	Period(d)	Mean V(mag)	B-V(mag)	J-K(mag)	Reference
V0508 And	ASASSN-V J004744.15+360223.3	0.7752302	12.11	0.390	0.254	Jayasinghe et al. (2019)
V0844 Aur	ASASSN-V J054305.62+530235.7	0.8222160	12.04	0.910	0.310	Jayasinghe et al. (2019)
V0699 Cep	ASASSN-V J224600.69+574649.6	0.8050727	11.72	0.859	0.394	Jayasinghe et al. (2019)
NSVS 6259046	ASASSN-V J232745.98+245256.9	0.7344176	12.69	0.550	0.309	Jayasinghe et al. (2019)

Table 2. The observating date, exposure time, comparison and check stars of the four investigated targets.

Target	Observing Date	Exposure Time (s)	Comparison Star	Check Star
V0508 And	2022 Nov 02,03,12,13,14	g22 i25 r20	TYC 2288-1478-1	Gaia DR3 364060257146400384
V0844 Aur	2021 Dec 26,30,31 2022 Jan 06,10,25	B40 V25 g20 r17 i22	TYC 3749-853-1	2MASS J05422180+5259148
V0699 Cep	2022 Sep 09,10,15,17,21,24	g15 i18 r12	GSC 03992-00111	TYC 3992-491-1
NSVS 6259046	2022 Sep 18-24, Oct 03	g32 i37 r27	2MASS J232731.469 +245741.655	Gaia DR3 2840468997644456192

Table 3. The photometric observation obtained by NEXT.

Target	HJD (2400000+)	Δm_B	HJD (2400000+)	Δm_V	HJD (2400000+)	Δm_g	HJD (2400000+)	Δm_r	HJD (2400000+)	Δm_i
V0508 And	-	-	-	-	59886.35012	-0.415	59886.35057	-0.346	59886.35099	-0.295
	-	-	-	-	...	...	...	...	...	...
V0844 Aur	59575.34264	-0.648	59575.34325	-0.687	59575.34373	-0.657	59575.34418	-0.715	59575.34459	-0.716
	...	...	...	...	...	...	...	...	...	...
V0699 Cep	-	-	-	-	59832.30586	-0.429	59832.30180	-0.443	59832.30212	-0.494
	-	-	-	-	...	...	...	...	...	...
NSVS 6259046	-	-	-	-	59841.34852	0.137	59841.34904	0.512	59841.34956	0.659
	-	-	-	-	...	...	...	...	...	...

Note. This table is available in its entirety in machine-readable form.

Table 4. Spectral observations of our targets from LAMOST.

Target	Observational date	Orbital Phase	Spectral type	$T_{\rm eff}$(K)	SNRg	[Fe/H]
V0508 And	2016-09-09	0.41	F5	6588 ± 13	253.30	0.117 ± 0.007
V0844 Aur	2014-02-10	0.98	F5	-	2.50	-
V0699 Cep	2014-12-02	0.35	F0	6660 ± 24	73.12	0.243 ± 0.021
NSVS 6259046	2013-10-15	0.27	F0	6642 ± 17	97.24	−0.083 ± 0.014

Table 5. Sources within 5 magnitudes and 42 arcsecs of our targets in Gaia DR3.

Target	Gaia Source ID	RA	Dec	RUWE	g mean flux (e^-/s)	g mean flux error (e^-/s)	g mean mag
V0508 And	364073176407230592	11.93397	36.03975	1.26	293920.45	1073.60	12.02
	364061429672596992	11.93335	36.02890	0.98	14057.75	3.78	15.32
	364073180703117696	11.92798	36.04014	1.09	6526.76	2.81	16.15
V0844 Aur	263713672034656000	85.77345	53.04316	1.02	319566.71	2112.52	11.93
	263713672035152512	85.77299	53.04748	0.94	9397.16	3.07	15.75
	263713710690720640	85.78852	53.04550	2.09	9243.48	7.58	15.77
	263713706394886656	85.78283	53.04506	0.94	9080.11	17.68	15.79
	263713676330987264	85.76471	53.03615	1.24	7285.53	9.96	16.03
V0699 Cep	2007362057959414144	341.50272	57.78044	1.78	348708.68	2259.62	11.83
	2007362062263640960	341.50306	57.78074	1.98	100942.60	48.10	13.18
	2007361684306521344	341.51398	57.78073	0.98	33056.56	41.72	14.39
	2007361306349403008	341.50580	57.76985	1.00	7903.99	3.00	15.94
	2007362062263637888	341.49361	57.78182	0.99	7077.66	4.07	16.06
	2007361684306520448	341.51335	57.78211	1.04	6272.52	2.36	16.19
	2007362440220762112	341.51681	57.78814	0.98	3891.32	2.22	16.71
NSVS 6259046	2840468276089961728	351.94181	24.88248	0.96	170505.10	689.82	12.61

is adjustable. By running the W-D program, convergent solutions are obtained after one iteration.

Three targets exhibit the O'Connell effect, which has four hypotheses to explain it. For circumstellar material and asymmetry of circumfluence from the Coriolis effect, the W-D code does not incorporate options to account for these mechanisms. Moreover, both hypotheses have been shown to suffer from significant shortcomings and are inadequate in explaining the O'Connell effect. For example, the authors who proposed the circumstellar material hypothesis, Liu & Yang (2003), themselves acknowledged that the model requires a specific geometric configuration and fails to consistently reproduce the observed O'Connell effect across multiple photometric bands. As a result, subsequent studies have generally regarded this explanation as limited in its applicability. Regarding the asymmetric circulation hypothesis, Wilsey & Beaky (2009) pointed out that this mechanism is not universally applicable to all types of binary systems, especially in detached or semi-detached systems. Moreover, this model has failed to successfully reproduce the observed light curve features in numerical simulations, further casting doubt on its validity. Now comes the hypothesis of cool spots and hot spot. For all targets, we test all possible combinations of cool spots and hot spots, and find that cool spots models provided the best explanation for their O'Connell effects. For V0699 Cep, we apply a cool spot to the secondary component. For V0844 Aur, we apply a cool spot to the primary component. In NSVS 6259046, initial attempts using a single cool or hot spot fail to provide a satisfactory fit to the light curve. Consequently, we introduce two spots and examine all four possible configurations involving cool and hot spots on either component. The best fit is achieved with a model incorporating a cool spot on the primary star and a hot spot on the secondary star.

Adalalı & Soydugan (2024) also performed photometric analysis on V0699 Cep. Apart from the third light contribution, the other parameters are generally consistent with our results. Since our value for the third light of V0699 Cep is consistent with the Gaia data shown in Table 5, this supports the accuracy of our study. For the other three targets, even with GAIA or O-C analysis, considering that the former is based on astrometric measurements and thus insensitive to smaller third-body orbits, while the latter is insensitive to face-on orbits of third bodies, we also attempt to add third light to these three targets. However, the results show that the proportion of third light is either negative or fails to converge to a solution. Therefore, we believe it is highly likely that these three targets do not exhibit third light. Future radial velocity observations may reveal whether these systems harbor third conponent. The photometric solutions for our four targets are detailed in Tables 6, 7, 8 and 9 respectively. The light curves observed by ASAS-SN, SuperWASP, TESS and ZTF are also analyzed by the W-D program. V0699 Cep is analyzed using TESS and ASAS-SN light curves, while data from TESS, ASAS-SN, and SuperWASP are utilized for V0844 Aur. For NSVS 6259046 and V0508 And, we collect data from ASAS-SN, SuperWASP, TESS and ZTF. For TESS data, V0699 Cep is observed in Sectors 16 and 17 and V0844 Aur is observed in Sectors 19, 59 and 73. Their light curves have significant differences between different sectors, so we analyze the different TESS sectors of these two targets separately. NSVS 6259046 is observed in Sector 56. V0508 And is observed in Sector 17 and 57. For V0508 And, there are no significant differences between the two light curves of Sectors 17 and 57, therefore we have merged them for analysis. We normalize the SAP-FLUX and convert the normalized flux to magnitude.

In the TESS, ASAS-SN, SuperWASP and ZTF studies, we initially set NEXT parameters as starting values. To improve program execution speed, TESS and SuperWASP data are binned into 200 normal points. Fig. 2 presents the theoretical light curves, while Tables 6 to 9 contain the photometric results. Additionally, all our four targets are totally eclipsing CBs, so the mass ratios obtained from the photometric observation is reliable (Pribulla et al. 2003c; Li et al. 2021). Some parameters differ among different surveys, especially the contact degree f, likely due to the difference in photometric accuracy among the surveys. We have selected the physical parameters derived from NEXT data as definitive solutions for our targets, due to the better multiband wavelength coverage. We also find that the mass ratios obtained from long-cadence TESS data are slightly lower than NEXT data, which is consistent with Zola et al. (2017). They demonstrated that long-cadence observations can distort the eclipse shape, particularly by altering the depth and width of minima, potentially leading to biased parameter estimates.

4 O - C ANALYSIS

Studying changes in orbital periods is crucial for understanding the dynamic interactions of binary systems, including the potential existence of a third body and how material transfers between the two components (Kim et al. 2006; Davis et al. 2014; Zhou et al. 2016b; Er-gang et al. 2019; Li et al. 2018; Liao et al. 2019; Pi et al. 2019). We gather as many times of minimum light as possible from our observations and photometric surveys, including data from NEXT, ASAS-SN, CRTS, TESS, SuperWASP, ZTF and $O-C$ Gateway.[2] Previous studies (Adalalı & Soydugan 2024) also analyzed V0699 Cep, and we have collected 4 eclipsing times from them. For NEXT, TESS and SuperWASP data, eclipsing times are calculated directly using the K–W method (Kwee & van Woerden 1956). A technique called period shift method (Li et al. 2020) is applied to determine the eclipsing times for CRTS, ASAS-SN, and ZTF, whose data points are relatively scarce and do not form a complete eclipsing curve. We convert the calculated eclipsing minimum from each survey to Barycentric Julian Date (BJD) through Time Utilities (Eastman et al. 2010).[3] Then, the following equation is used to find the calculated times,

$$Min.I = Min.I_0 + P \times E, \quad (3)$$

where $Min.I$ and $Min.I_0$ denote the observed minimum and initial epoch, respectively, and E represents the cycle number. Table 10 presents all eclipsing times and $O-C$ values. Fig. 3 displays the $O-C$ diagrams of the four targets. V0699 Cep, NSVS 6259046 and V0508 And show distinct parabolic trends, for which the following equation is used to fit their $O-C$ curves,

$$O - C = \Delta Min.I_0 + \Delta P \times E + \frac{\beta}{2} \times E^2, \quad (4)$$

where $\Delta Min.I_0$ represents the adjustment made to the initial epoch, ΔP denotes a correction applied to the orbital period, and β signifies the long-term orbital period changes rate. The outcomes are listed in Table 11. The positive β indicates that the orbital periods of V0699 Cep, NSVS 6259046 and V0508 And are all increasing in the long term. Conversely, there is no evidence toward a parabolic tendency for V0844 Aur, we linearly fit its $O-C$ curve.

[2] https://var.astro.cz/en
[3] https://astroutils.astronomy.osu.edu/time/

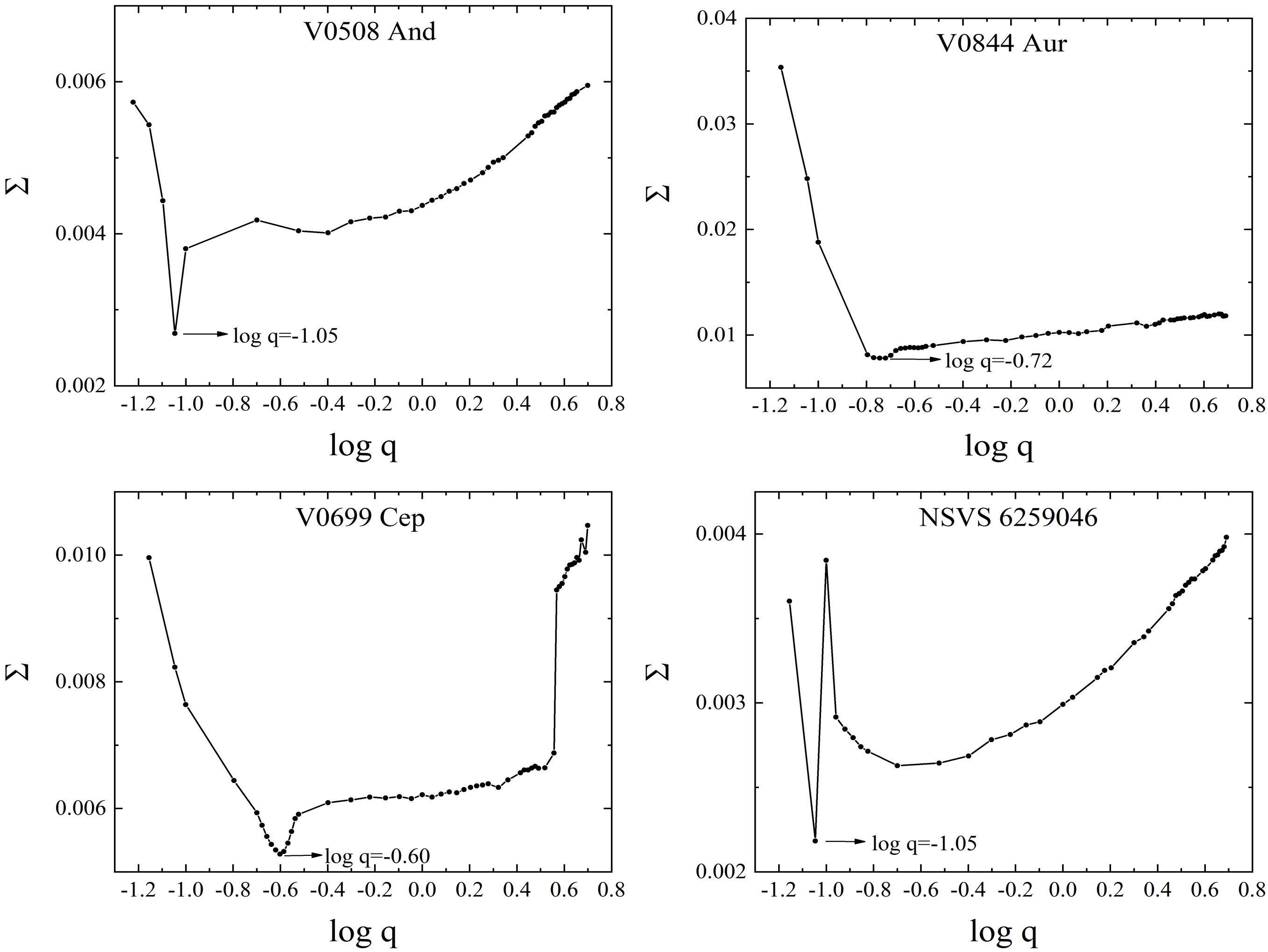

Figure 1. The relation between mass ratio q and mean residual Σ generated by the W-D program for the NEXT light curves, the mass ratios are ranging from 0.06 to 5.00.

5 SPECTRAL ANALYSIS

The emission lines in the spectrum such as H_α, H_β, Ca II H&K and IRT, etc. can serve as reliable indicators of chromospheric activity (Wilson 1978; Barden et al. 1984; Montes et al. 1995). According to Table 4, we choose V0699 Cep, NSVS 6259046 and V0508 And, whose signal-to-noise ratios are high enough for us to analyze. The observed spectrum of a star, however, generally exhibits absorption in the H_α line, which is attributed to the stellar photosphere's absorption. Thus, we use the spectral subtraction method according to Barden (1985), removing photospheric spectrum from the observed spectrum to obtain pure chromospheric spectrum. First, we select spectra of two inactive stars for each system from the catalog of Zhang et al. (2021), ensuring that the temperature difference between the inactive stars and the target was less than 200 K. One spectrum is used as the primary template, while the other served as the secondary template. After downloading and normalizing the spectra, we apply the STARMOD code (Barden 1985) to generate synthetic spectrum for the two inactive stars, considering radial velocities, spin angular velocities, and the luminosity ratios of the components. Next we obtain the subtracted spectra from the synthetic spectra and the target spectra, and the results are shown in Fig. 4. For NSVS 6259046 and V0508 And, there is no H_α emission line, which indicates no chromospheric activity for these two targets. Only V0699 Cep shows clear H_α emission lines, suggesting it possesses chromospheric activity. So we calculate its equivalent width (EW) of the H_α line using package of the IRAF to further quantify its chromospheric activity. The EW is found out to be 0.41 Å. The EW of H_α for other CBs with $T_{\rm eff}$ higher than 5900 K are presented in Table 12. The comparative analysis shows that V0699 Cep displays a relatively high degree of chromospheric activity among early-type stars.

6 DISCUSSION AND CONCLUSION

We conduct a photometric and spectroscopic investigation of four CBs with period longer than 0.7 days. The reliability of our photometric results is supported by the characteristic flat secondary eclipsing minima, as earlier studies have demonstrated that in the absence of large unidentified third light, the photometric and spectroscopic methods yield nearly equal mass ratios for totally eclipsing contact binaries (Pribulla et al. 2003a; Terrell & Wilson 2005; Li et al. 2021).

The contact degree (f) serves as a key criterion for classifying contact binary systems into deep, medium, and shallow contact categories. A system is classified as deep contact if $f \geq 50\%$, medium contact if $25\% \leq f < 50\%$, and shallow contact if $f < 25\%$ (Qian

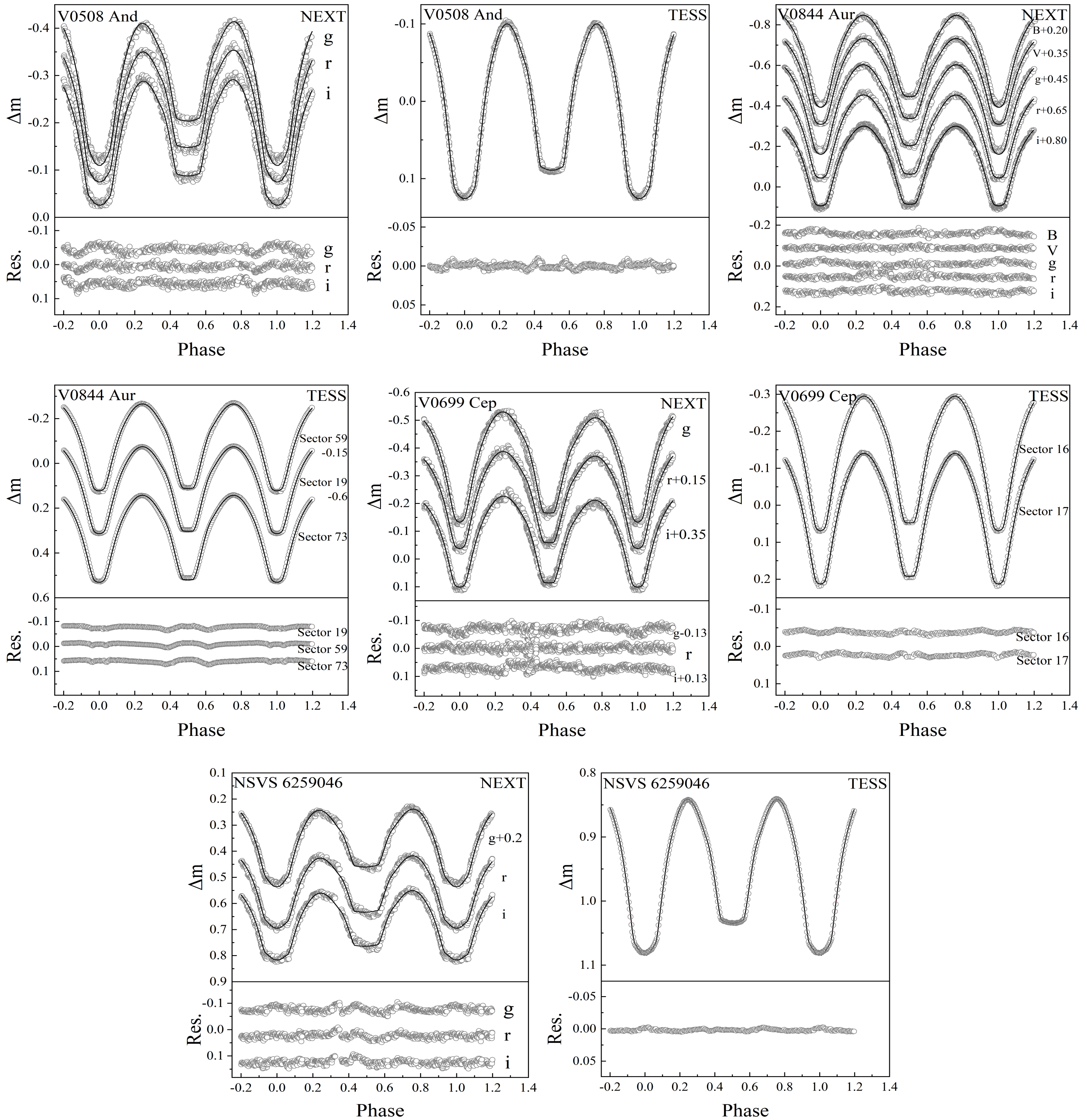

Figure 2. This figure presents a comparison between the observed (symbols) and theoretical (solid lines) light curves generated by the W-D program for the NEXT, TESS, ASAS-SN, SuperWASP and ZTF light curves. The residuals of the fit are also displayed.

et al. 2005; Liu et al. 2023). V0699 Cep (f = 37.3%), V0844 Aur (f = 37.7%) and V0508 And (f = 43.2%) are found to be medium-contact binaries, while NSVS 6259046 (f = 64.4%) is found to be a deep-contact binary. The four targets are classified as A-type CBs due to the positive correlation between the mass and temperature of the primary and secondary components (Binnendijk 1970). Although chromospheric activity usually exists in the kind of systems with spectral type later than F (Eker et al. 2008b), we find obvious chromospheric activity on V0699 Cep.

6.1 O'Connell Effect and Magnetic Activity

During the analysis of the light curves, we find that V0844 Aur, V0699 Cep and NSVS 6259046 exhibit O'Connell effect, with the fraction of the magnitude difference between the two maxima relative to the total amplitude (depth of primary minimum) being 2.7%, 11.6%, and 7.9%, respectively. In late-type CBs, the asymmetry in the light-curve maxima, known as the O'Connell effect, is typically explained by the presence of dark spots. This phenomenon is attributed to rapid differential rotation and the large convective zone (Pribulla

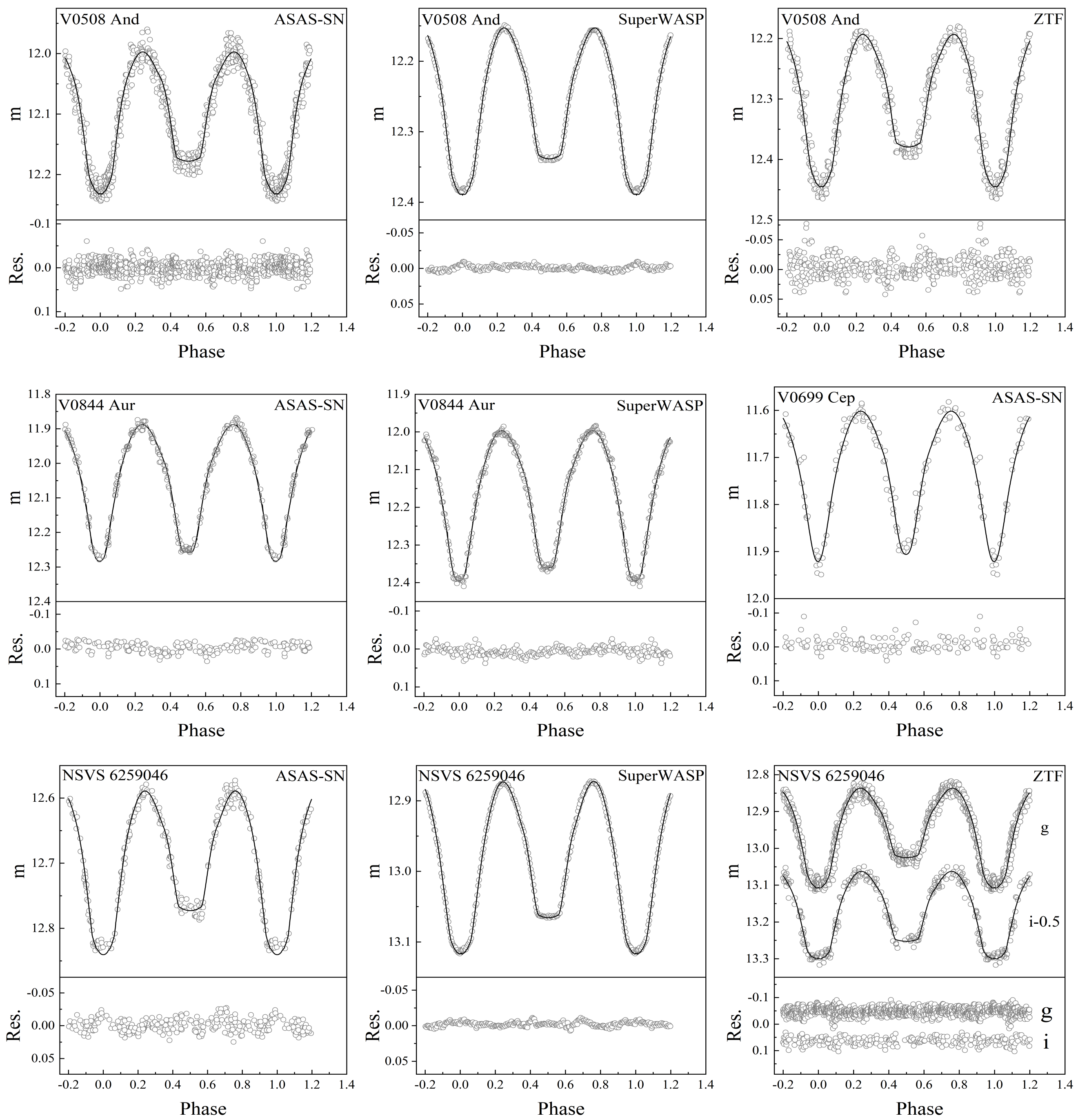

Figure 2. (Continued)

et al. 2011). Theoretically, most early-type CBs display symmetric light curves. However, several studies have shown that, despite the absence of convective zones, a significant O'Connell effect can still be observed in some early-type CBs (Pribulla et al. 2011; Knote et al. 2022). All of our four targets are early-type systems, three of them exhibit O'Connell effect. For V0844 Aur and V0699 Cep, the 0.25-phase maximum is brighter than the 0.75-phase maximum in the NEXT data. As for NSVS 6259046, the 0.75-phase maximum is brighter than the 0.25-phase maximum in the NEXT and SuperWASP data. But in the TESS data, their maxima are all equal. We conclude that these three targets all show variable O'Connell effect. Due to the poor quality of ASAS-SN and ZTF data, the O'Connell effect could not be identified in these datasets. Overall, we infer that these targets exhibit strong magnetic activity. Our study provides evidence supporting that even in early-type systems lacking convective zones, the O'Connell effect can still be present. The relatively weaker O'Connell effect observed in V0844 Aur and NSVS 6259046 compared to V0699 Cep suggests that their magnetic activity may also be less intense. This is consistent with our finding that chromospheric activity is only detected in V0699 Cep. Moreover, the photometric and spectroscopic observations were not conducted simultaneously; therefore, it is possible that the O'Connell effect

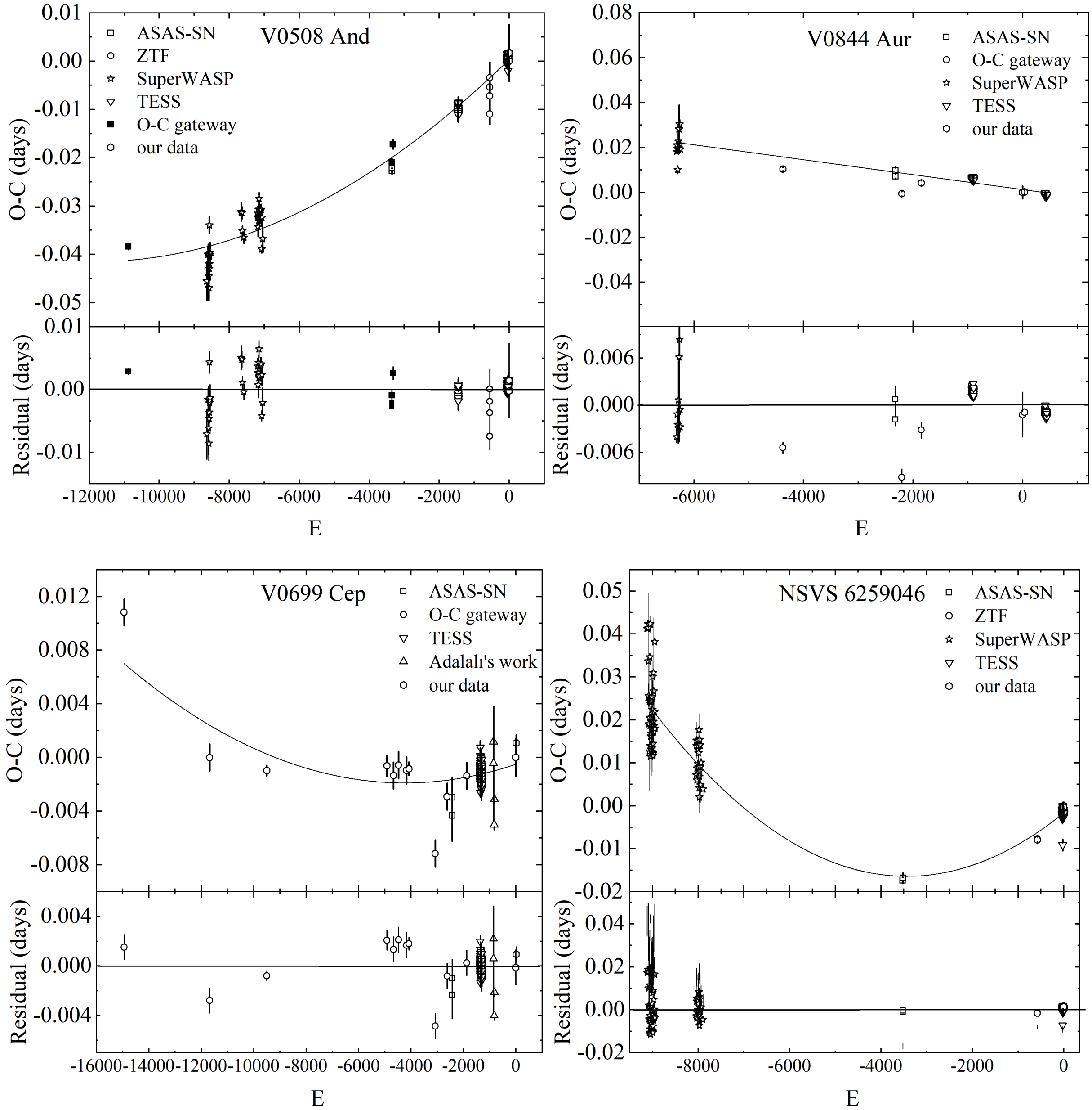

Figure 3. The upper illustration shows the $O-C$ diagram and the lower illustration refers to the residuals. Eclipsing times are from NEXT, ASAS-SN, CRTS, TESS, SuperWASP, ZTF, $O-C$ Gateway and Adalalı & Soydugan (2024).

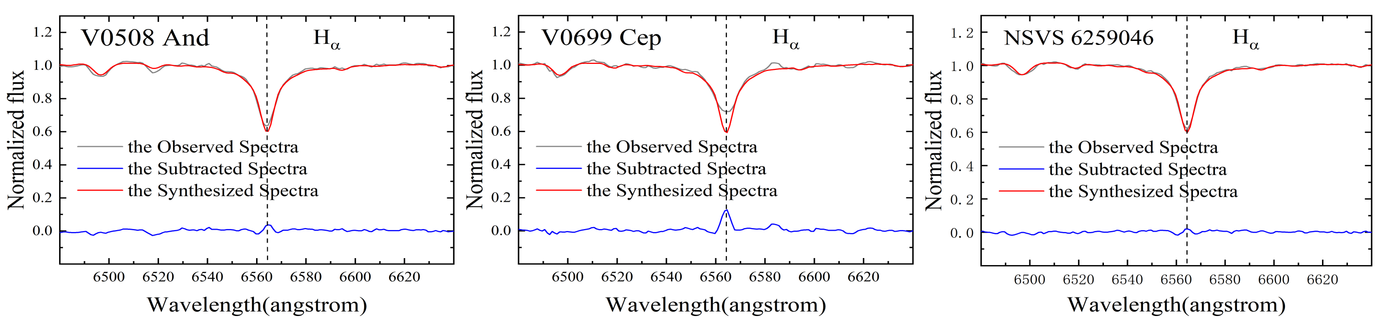

Figure 4. The normalized observed, synthesized, and subtracted spectra near the location of H_α observed by LAMOST.

Table 6. Photometric solutions of V0699 Cep

Parameter	NEXT	TESS	ASAS-SN
T_1 (K)	6660 ± 31	6662 ± 31	6666 ± 44
T_2 (K)	6659 ± 56	6651 ± 57	6641 ± 119
q (M_1/M_2)	0.240 ± 0.002	0.225 ± 0.001	0.240 ± 0.002
i (°)	80.3 ± 0.2	78.8 ± 0.1	77.1 ± 3.0
Ω	2.274 ± 0.003	2.229 ± 0.003	2.286 ± 0.017
r_1	0.524 ± 0.001	0.534 ± 0.001	0.523 ± 0.005
r_2	0.282 ± 0.004	0.284 ± 0.003	0.281 ± 0.007
$L_2/(L_1+L_2+L_3)$ (g)	0.187 ± 0.030	-	-
$L_3/(L_1+L_2+L_3)$ (g)	0.163 ± 0.005	-	-
$L_2/(L_1+L_2+L_3)$ (r)	0.177 ± 0.036	-	-
$L_3/(L_1+L_2+L_3)$ (r)	0.205 ± 0.004	-	-
$L_2/(L_1+L_2+L_3)$ (i)	0.173 ± 0.039	-	-
$L_3/(L_1+L_2+L_3)$ (i)	0.224 ± 0.004	-	-
$L_2/(L_1+L_2+L_3)$ (TESS-Sector 16)	-	0.184 ± 0.026	-
$L_3/(L_1+L_2+L_3)$ (TESS-Sector 16)	-	0.139 ± 0.003	-
$L_2/(L_1+L_2+L_3)$ (TESS-Sector 17)	-	0.180 ± 0.029	-
$L_3/(L_1+L_2+L_3)$ (TESS-Sector 17)	-	0.162 ± 0.003	-
$L_2/(L_1+L_2+L_3)$ (V)	-	-	0.169 ± 0.043
$L_3/(L_1+L_2+L_3)$ (V)	-	-	0.254 ± 0.034
f (%)	37.3 ± 2.2	45.1 ± 1.9	-
Cool Spot	Star 2	-	-
$\theta°$	135 ± 1	-	-
$\lambda°$	288 ± 3	-	-
$r_{\rm spot}$	33 ± 1	-	-
$T_{\rm spot}$	0.787 ± 0.014	-	-

Table 7. Photometric solutions of V0844 Aur

V0844 Aur	NEXT	TESS	ASAS-SN	SuperWASP
T_1 (K)	6642 ± 239	6537 ± 244	6540 ± 244	6556 ± 241
T_2 (K)	6130 ± 408	6604 ± 448	6591 ± 443	6521 ± 440
q (M_1/M_2)	0.198 ± 0.001	0.193 ± 0.001	0.198 ± 0.001	0.177 ± 0.003
i (°)	78.8 ± 0.2	78.4 ± 0.2	77.1 ± 0.6	77.5 ± 0.6
Ω	2.180 ± 0.004	2.159 ± 0.002	2.144 ± 0.005	2.122 ± 0.008
r_1	0.539 ± 0.001	0.545 ± 0.001	0.546 ± 0.002	0.551 ± 0.002
r_2	0.267 ± 0.004	0.269 ± 0.003	0.262 ± 0.002	0.264 ± 0.011
$L_2/(L_1+L_2)$ (B)	0.129 ± 0.002	-	-	-
$L_2/(L_1+L_2)$ (V)	0.144 ± 0.001	-	0.183 ± 0.002	-
$L_2/(L_1+L_2)$ (g)	0.135 ± 0.001	-	-	-
$L_2/(L_1+L_2)$ (r)	0.150 ± 0.001	-	-	-
$L_2/(L_1+L_2)$ (i)	0.158 ± 0.001	-	-	-
$L_2/(L_1+L_2)$ (TESS-Sector 19)	-	0.198 ± 0.001	-	-
$L_2/(L_1+L_2)$ (TESS-Sector 59)	-	0.198 ± 0.001	-	-
$L_2/(L_1+L_2)$ (TESS-Sector 73)	-	0.198 ± 0.001	-	-
$L_2/(L_1+L_2)$ (SuperWASP)	-	-	-	0.180 ± 0.002
f (%)	37.7 ± 2.9%	45.4 ± 1.8%	40.0 ± 4.3%	46.9 ± 7.0%
Cool Spot	Star 1	-	-	-
$\theta°$	125 ± 1	-	-	-
$\lambda°$	179 ± 0	-	-	-
$r_{\rm spot}$	22 ± 0	-	-	-
$T_{\rm spot}$	0.738 ± 0.008	-	-	-

was detected photometrically while no chromospheric activity was observed spectroscopically.

6.2 Statistics of 217 CBs and Absolute Parameters Calculation

We compile a dataset of 217 CBs with both reliable radial velocity and photometric observations shown in Table A1. We divide A-type and W-type CBs into two groups and investigate their period distributions separately, which is shown in Fig. 5. We find that A-type systems systematically have longer orbital periods than W-type systems.

To assess the evolutionary status of the our targets, we calculate their absolute physical parameters. In order to achieve that, we first calculate the distance between the two components by using the orbital period and semimajor axis (P–a) empirical relationship. However, most of the previous work established this relationship based on CBs with periods shorter than 0.7 days (e.g. Poro et al. 2024c),

$$a = \left(0.372^{+0.113}_{-0.114}\right) + \left(5.914^{+0.272}_{-0.298}\right) \times P. \quad (5)$$

Table 8. Photometric solutions of NSVS 6259046

NSVS 6259046	NEXT		TESS	ASAS-SN	SuperWASP	ZTF
T_1 (K)	6677 ± 22		6699 ± 20	6698 ± 21	6655 ± 19	6699 ± 24
T_2 (K)	6360 ± 21		6140 ± 18	6360 ± 21	6528 ± 19	6127 ± 22
q (M_1/M_2)	0.090 ± 0.001		0.091 ± 0.000	0.090 ± 0.001	0.064 ± 0.000	0.093 ± 0.001
i (°)	85.3 ± 0.2		83.8 ± 0.1	84.0 ± 1.0	75.1 ± 0.2	83.8 ± 0.3
Ω	1.889 ± 0.003		1.903 ± 0.001	1.910 ± 0.002	1.798 ± 0.000	1.921 ± 0.005
r_1	0.606 ± 0.001		0.600 ± 0.001	0.597 ± 0.001	0.637 ± 0.000	0.594 ± 0.002
r_2	0.221 ± 0.008		0.215 ± 0.003	0.207 ± 0.001	0.216 ± 0.001	0.210 ± 0.008
$L_2/(L_1+L_2)$ (g)	0.090 ± 0.001		-	-	-	0.072 ± 0.001
$L_2/(L_1+L_2)$ (r)	0.096 ± 0.001		-	-	-	0.086 ± 0.001
$L_2/(L_1+L_2)$ (i)	0.099 ± 0.001		-	-	-	-
$L_2/(L_1+L_2)$ (SuperWASP)	-		-	-	0.086 ± 0.001	-
$L_2/(L_1+L_2)$ (TESS-Sector 56)	-		0.087 ± 0.000	-	-	-
$L_2/(L_1+L_2)$ (V)	-		-	0.074 ± 0.002	-	-
f (%)	64.4 ± 4.7%		46.7 ± 2.3%	-	-	-
Cool and Hot Spot	Star 1 (Cool Spot)	Star 2 (Hot Spot)	-	-	Star 2 (Cool Spot)	-
θ°	174 ± 1	40 ± 4	-	-	43 ± 2	-
λ°	140 ± 7	151 ± 8	-	-	178 ± 2	-
$r_{\rm spot}$	33 ± 1	33 ± 1	-	-	32 ± 1	-
$T_{\rm spot}$	0.802 ± 0.011	1.202 ± 0.023	-	-	0.802 ± 0.015	-

Table 9. Photometric solutions of V0508 And

Parameter	NEXT	TESS	ASAS-SN	SuperWASP	ZTF
T_1 (K)	6624 ± 17	6626 ± 15	6624 ± 16	6620 ± 16	6623 ± 23
T_2 (K)	6292 ± 37	6233 ± 28	6237 ± 44	6279 ± 30	6251 ± 57
q (M_1/M_2)	0.094 ± 0.001	0.088 ± 0.000	0.094 ± 0.001	0.080 ± 0.000	0.085 ± 0.002
i (°)	84.3 ± 0.2	83.2 ± 0.1	85.0 ± 0.2	79.3 ± 0.2	85.1 ± 0.4
Ω	1.915 ± 0.003	1.909 ± 0.000	1.927 ± 0.002	1.877 ± 0.002	1.901 ± 0.010
r_1	0.597 ± 0.001	0.596 ± 0.000	0.589 ± 0.001	0.607 ± 0.001	0.598 ± 0.004
r_2	0.216 ± 0.006	0.204 ± 0.001	0.198 ± 0.001	0.203 ± 0.005	0.202 ± 0.019
$L_2/(L_1+L_2)$ (g)	0.090 ± 0.001	-	-	-	0.074 ± 0.003
$L_2/(L_1+L_2)$ (r)	0.096 ± 0.001	-	-	-	-
$L_2/(L_1+L_2)$ (i)	0.099 ± 0.002	-	-	-	-
$L_2/(L_1+L_2)$ (TESS)	-	0.088 ± 0.000	-	-	-
$L_2/(L_1+L_2)$ (V)	-	-	0.079 ± 0.001	-	-
$L_2/(L_1+L_2)$ (SuperWASP)	-	-	-	0.077 ± 0.001	-
f (%)	43.2 ± 4.1%	22.4 ± 0.9%	-	37.0 ± 4.1%	-

Table 10. The Eclipsing times and $O-C$ values of the four targets.

Targets	BJD (2400000+)	E	$O-C$ (days)	Residual (days)	Source
V0508 And	51464.04070	-10880	-0.03839	0.00040	O-C gateway
	...	...	...	...	...
V0844 Aur	54382.68684	-6315.5	0.01816	0.00068	SuperWASP
	...	...	...	...	...
V0699 Cep	47804.39825	-14941.5	0.01082	0.00100	O-C gateway
	...	...	...	...	...
NSVS 6259046	53153.69265	-9117	0.04125	0.00700	SuperWASP
	...	...	...	...	...

Note. This table is available in its entirety in machine-readable form.

Among our four systems, none have an orbital period shorter than 0.7 days. To determine their absolute parameters more accurately, we use 44 CBs in Table A1 to determine a new P–a relationship for long-period contact binaries. Given the limited number of CBs with periods longer than 0.7 days, we perform the fitting using systems with period of 0.5–1.0 range to enhance the reliability of the fit.

Regarding the fitting approach, since Kepler's third law is a power law relationship between a and P, we apply a logarithmic trans-

Table 11. Fitting parameters including rates of period variation and mass transfer of the four CBs by $O-C$ analysis.

Targets	$\Delta Min.I_0$ ($\times10^{-4}$ d)	Error ($\times10^{-4}$ d)	ΔP ($\times10^{-7}$ d)	Error ($\times10^{-7}$ d)	β ($\times10^{-7}$ d yr^{-1})	Error ($\times10^{-7}$ d yr^{-1})	$\frac{dM_1}{dt}$ ($\times10^{-8} M_\odot$ yr^{-1})
V0508 And	2.7	2.6	70.5	2.8	2.8	0.3	2.9
V0844 Aur	12.2	2.0	−33.3	1.1	–	–	–
V0699 Cep	−5.3	2.7	6.6	2.2	0.7	0.2	1.9
NSVS 6259046	−17.6	5.9	85.7	10.8	12.4	1.2	12.6

Table 12. The H_α EW of other CBs with $T_{\rm eff}$ higher than 5900 K. We find that V0699 Cep exhibits a larger H_α EW compared to other CBs with $T_{\rm eff}$ higher than 5900 K.

Star	UT Date	SNR	Spectral type	$T_{\rm eff}$ (K)	H_α (Å)	Ref.
J001422.52+415331.1	2013 Nov 14	279	F0	6568(±9)	0.294(±0.006)	(1)
J022733.60+360447.1	2017 Jan 06	174	F5	6477(±9)	0.252(±0.003)	(1)
J040927.64+463400.6	2012 Dec 21	157	A7	7106(±25)	0.761(±0.005)	(2)
J042640.22+370047.7	2013 Feb 02	2	–	–	–	(1)
	2013 Oct 04	55	F7	5936(±41)	0.285(±0.021)	
	2013 Oct 04	89	F6	6054(±18)	0.223(±0.011)	
	2015 Jan 12	148	F6	6115(±14)	0.368(±0.037)	
J054950.33+584208.9	2013 Feb 18	71	F0	6988(±30)	0.239(±0.019)	(1)
	2013 Dec 27	131	F0	6987(±15)	0.223(±0.009)	
J062623.89+275644.2	2012 Feb 29	172	F0	7072(±16)	0.011(±0.004)	(2)
J110658.46+511200.1	2013 Dec 21	203	F5	6252(±12)	0.372(±0.022)	(1)
	2015 Dec 30	233	F6	6255(±11)	0.323(±0.030)	
	2016 Jan 28	121	F7	6195(±20)	0.200(±0.018)	
J115742.23+074820.3	2014 May 22	56	F5	5997(±47)	0.202(±0.013)	(1)
J153433.52+122516.7	2015 Feb 13	14	F6	6077(±366)	0.638(±0.065)	(1)
J190254.60+395028.6	2020 Sep 21	55	F5	6454(±49)	0.240(±0.006)	(2)
J192211.74+492834.2	2016 Dec 11	386	F0	7307(±7)	0.007(±0.004)	(2)
J192728.90+421943.1	2013 May 20	106	F5	6619(±28)	0.104(±0.005)	(2)
J233332.90+180429.9	2014 Oct 13	73	F0	6728(±27)	0.301(±0.026)	(1)
HAT 307-0007476	2015 Dec 20	20	F0	6843(±68)	0.373(±0.016)	(3)
	2015 Dec 27	24	F0	6821(±64)	0.258(±0.031)	
	2016 Jan 12	30	A9	6820(±155)	0.296(±0.025)	
	2016 Nov 04	56	F0	6895(±35)	0.303(±0.005)	
V342 UMa	2022 Feb 24	22	F7	5923(±109)	0.096(±0.048)	(4)

References. (1)Li et al. (2022a), (2)Shi et al. (2025), (3)Li et al. (2025), (4)Zhang et al. (2025).

formation to them. According to the diagram, we perform a linear regression in log-log space.

A relationship is determined in Fig. 6, which is shown as follows:

$$\log a = (0.786 \pm 0.014) + (0.901 \pm 0.072) \times \log P. \quad (6)$$

A direct comparison between our newly derived relation and that of Poro et al. (2024c) is carried out. We quantitatively evaluate the performance by calculating the residual sum of squares (RSS) for the two models against the 44 long-period systems. The result shows that our log-log fit achieves a smaller RSS of 0.0582, while the relation from Poro et al. (2024c) produces a larger RSS of 0.0611. Their relation, while well-suited for its original short-period sample ($P < 0.5$ days), shows systematic deviations when applied to the long-period regime ($P > 0.5$ days). The smaller RSS value indicates that the log-log fit is a more suitable relation for long-period regime.

Therefore, we calculate the semimajor axes of our four long period binary systems using this linear fit in log-log space. The relative radii and semimajor axis are then used to determine R_1 and R_2. According to Kepler's third law, the total mass of the system is given by:

$$M_1 + M_2 = \frac{0.0134a^3}{P^2}. \quad (7)$$

Then we use the mass ratio q to determine the primary mass M_1 and the secondary mass M_2. M, a, and P are expressed in solar masses ($M_\odot$), solar radii ($R_\odot$), and days, respectively. Next, the luminosities L_1 and L_2 are derived using the Stefan-Boltzmann law:

$$L = 4\pi\sigma T^4 R^2. \quad (8)$$

The absolute parameters of our targets are summarized in Table 13.

The orbital periods of V0508 And, V0699 Cep, and NSVS 6259046 are increasing continuously, while that of V0844 Aur may remain unchanged at present. As the Applegate mechanism is generally associated with periodic or quasi-periodic $O-C$ variations (Applegate 1992; Völschow et al. 2016; Li & Hong 2018), and our targets show no evidence of such periodic variations, the observed long-term period change is more consistent with a mass transfer scenario. The long-term increase in orbital period could be caused by mass transfer from the less massive star to the more massive one (Zhu et al. 2011; Kudak et al. 2021; Guo et al. 2022; Li et al. 2022a; Gao et al. 2022; Matekov et al. 2023; Zervas et al. 2024; Liu et al. 2024; Li et al. 2025). Based on this assumption, we use the following equation to estimate the rate of mass transfer:

$$\frac{dM_1}{dt} = \frac{M_1 M_2}{3P(M_1 - M_2)} \times \frac{dP}{dt}. \quad (9)$$

The final values are displayed in Table 11.

Table 13. Absolute parameters of the four targets by the P–a empirical relation method and the Gaia distance method.

Targets [a]	RUWE	A_v	Gaia Distance (kpc)	a ($R_\odot$)	M_1 ($M_\odot$)	M_2 ($M_\odot$)	R_1 ($R_\odot$)	R_2 ($R_\odot$)	L_1 ($L_\odot$)	L_2 ($L_\odot$)
V0508 And(P–a empirical relation)	–	–	–	4.86(±0.18)	2.34(±0.26)	0.22(±0.03)	2.90(±0.11)	1.05(±0.07)	14.52(±1.12)	1.55(±0.20)
V0508 And(Gaia distance)	1.26	0.13	0.98	4.78(±0.08)	2.22(±0.12)	0.21(±0.01)	2.85(±0.05)	0.99(±0.04)	14.05(±0.48)	1.47(±0.07)
V0844 Aur(P–a empirical relation)	–	–	–	5.13(±0.18)	2.23(±0.24)	0.44(±0.05)	2.76(±0.10)	1.37(±0.07)	13.32(±0.99)	2.37(±0.30)
V0844 Aur(Gaia distance)	1.02	0.76	0.91	5.96(±0.21)	3.50(±0.36)	0.69(±0.08)	3.21(±0.12)	1.59(±0.08)	18.15(±0.47)	3.04(±0.11)
V0699 Cep(P–a empirical relation)	–	–	–	5.03(±0.18)	2.12(±0.23)	0.51(±0.06)	2.63(±0.10)	1.42(±0.07)	12.23(±0.91)	3.54(±0.36)
V0699 Cep(Gaia distance)	1.78	0.82	0.75	5.91(±0.10)	3.45(±0.17)	0.83(±0.05)	3.10(±0.06)	1.67(±0.05)	16.94(±0.57)	4.86(±0.27)
NSVS 6259046(P–a empirical relation)	–	–	–	4.63(±0.18)	2.26(±0.27)	0.20(±0.03)	2.81(±0.12)	1.02(±0.08)	14.03(±1.15)	1.54(±0.23)
NSVS 6259046(Gaia distance)	0.96	0.43	1.12	4.67(±0.08)	2.32(±0.12)	0.21(±0.01)	2.66(±0.05)	1.03(±0.05)	14.33(±0.46)	1.51(±0.06)

Note. [a] Errors were estimated in terms of error transfer formulae.

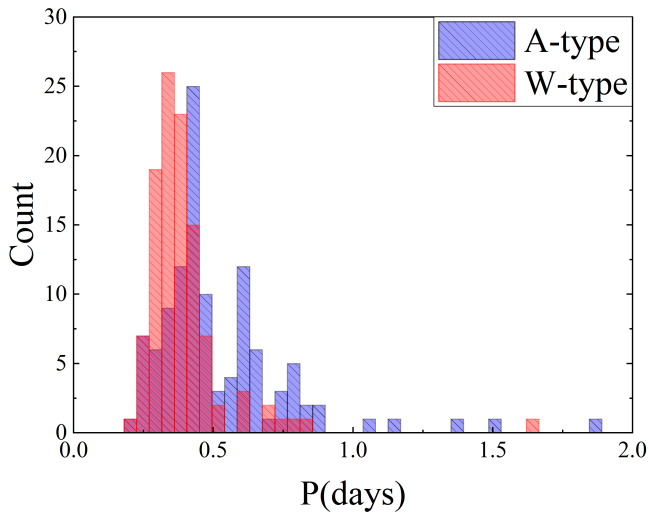

Figure 5. The orbital period distribution of A-type and W-type CBs from the statistical analysis of 217 systems.

In addition to the P–a empirical relation method, there is another approach that utilizes Gaia distances to calculate absolute parameters.

Following the research by Li et al. (2021), we employ the equation:

$$M_v = m_{v\,\max} - 5\log D + 5 - A_v \tag{10}$$

to calculate the absolute magnitudes (M_v), where A_v represents the extinction coefficients, $m_{v\,\max}$ denotes the brightest V-band magnitude from the ASAS-SN theoretical curve, and D is the distance provided by Gaia DR3 (Gaia Collaboration et al. 2016, 2023). The bolometric corrections (BC_v) are then derived through interpolation from the table given by Pecaut & Mamajek (2013). The absolute bolometric magnitude $M_{\rm bol}$ is given by:

$$M_{\rm bol} = M_v + BC_v. \tag{11}$$

From the relation

$$M_{\rm bol} = -2.5\log\left(\frac{L_{\rm total}}{L_\odot}\right) + 4.75, \tag{12}$$

we derive the luminosities for the primary and secondary components ($L_{1,2}$). The equation:

$$M_{\rm bol} = -2.5\log\left[(A\times r_1)^2\left(\frac{T_1}{T_\odot}\right)^4 + (A\times r_2)^2\left(\frac{T_2}{T_\odot}\right)^4\right] + 4.75 \tag{13}$$

is applied to compute the distance (A) between the two components, where r_1 and r_2 are the relative radii of the primary and secondary components from the photometric solutions. Using

$$\frac{R_1}{R_\odot} = r_1\times A \quad \text{and} \quad \frac{R_2}{R_\odot} = r_2\times A, \tag{14}$$

the radii of the primary and secondary components ($R_{1,2}$) in solar units are determined. Finally, by using Kepler's third law

$$M_1 + M_2 = 0.0134\frac{A^3}{P^2}, \tag{15}$$

where P is in days and A is in solar units ($R_\odot$), the total mass of the system is obtained. The mass ratio from the W-D program is then used to estimate the masses of the primary and secondary ($M_{1,2}$). The absolute parameters along with their errors are presented in Table 13.

However, to ensure the accuracy of the calculated absolute physical parameters, the RUWE must remain below 1.4 (Poro et al. 2024c) and A_v should not exceed approximately 0.4 (Poro et al. 2024b). We have listed the RUWE and A_v of each target in Table 14. Due to that V0699 Cep exhibits a RUWE > 1.4 and Av > 0.4, while V0844 Aur also shows Av > 0.4, the absolute physical parameters of V0699 Cep and V0844 Aur calculated using the Gaia distance may be less accurate than those obtained with the P–a empirical relation. Meanwhile, the results from the Gaia distance method for V0508 And and NSVS 6259046 are consistent with those obtained from the P–a empirical relation method. Therefore, the absolute parameters given by the P–a empirical relation are chosen as the final results.

6.3 Initial Mass and Age

We determine the initial mass and mass ratio of each component using the equations proposed by Yildiz & Doğan (2013):

$$M_{2i} = M_2 + \Delta M = M_2 + 2.50(M_L - M_2 - 0.07)^{0.64}, \tag{16}$$

where M_2 denotes the present mass of the secondary star, while M_L is obtained from:

$$M_L = \left(\frac{L_2}{1.49}\right)^{1/4.216}. \tag{17}$$

The initial mass of the primary star is derived as:

$$M_{1i} = M_1 - (\Delta M - M_{\rm lost}) = M_1 - \Delta M(1-\gamma), \tag{18}$$

where M_1 represents the current mass of the primary, and the total mass lost by the system is denoted as $M_{\rm lost}$. The parameter γ is defined by:

$$\gamma = \frac{M_{\rm lost}}{\Delta M}. \tag{19}$$

$\gamma = 0$ corresponds to the conservative case and $\gamma = 1$ corresponds to the case that the mass loss by the primary star is 0. In our calculations, we adopt $\gamma = 0.664$, following Yildiz & Doğan (2013).

$$q_{\rm ini} = \frac{M_{2i}}{M_{1i}}, \tag{20}$$

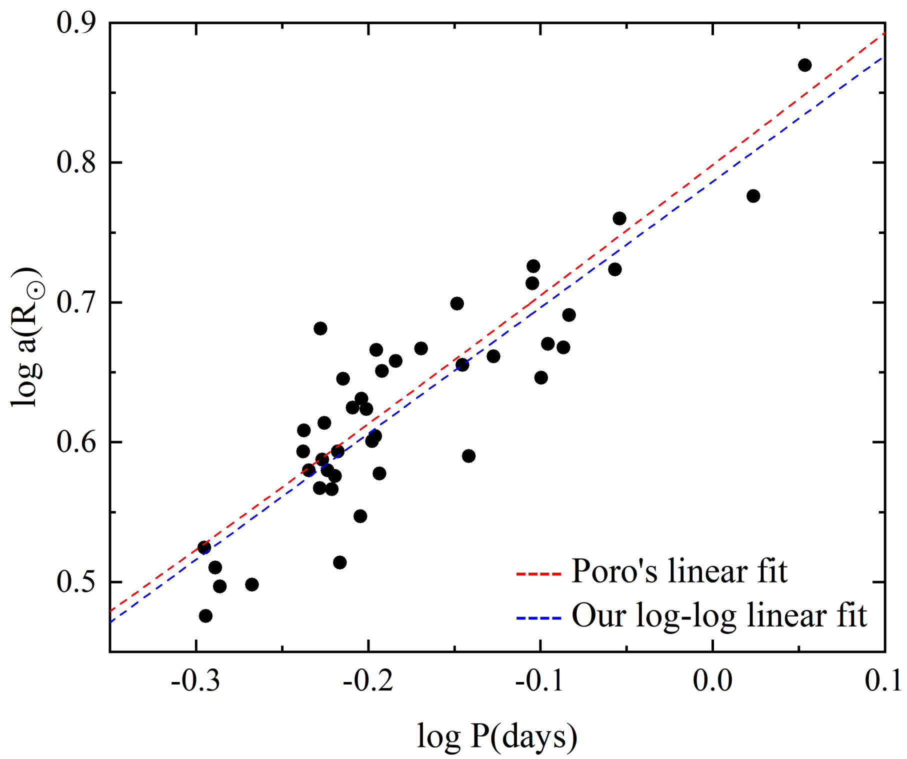

Figure 6. Black solid dots represent a sample of 44 CBs with P > 0.5 days selected from 217 systems. Dashed line represents the relationship between the period P and the semimajor axis a. Blue represents our linear fit in log-log space using this sample. Red represents the linear relationship established by Poro et al. (2024c) using samples with P < 0.7 days, which is expressed in logarithmic form and incorporated into the figure. We have calculated the residual sum of squares for the two methods across the 44 long-period CBs. The residual sum of squares is 0.0582 for our log-log fit, and 0.0611 for Poro's linear fit. With the smaller residual sum of squares, the log-log fit proves to be more suitable for the long-period regime.

Table 14. The initial mass, age, orbital angular momentum and stability parameter of the four targets.

Targets	M_{1i} (M$_\odot$)	M_{2i} (M$_\odot$)	$q_{\rm ini}$	t (Gyr)	J_o (cgs)	$\frac{J_s}{J_o}$
V0508 And	1.66	2.24	1.35	2.59	4.307×10^{51}	0.152
V0844 Aur	1.62	2.25	1.39	2.38	8.240×10^{51}	0.077
V0699 Cep	1.49	2.40	1.62	1.91	9.024×10^{51}	0.067
NSVS 6259046	1.57	2.26	1.43	2.56	3.809×10^{51}	0.162

Here, M_{1i} and M_{2i} are the present masses of the primary and secondary stars, respectively, while $q_{\rm ini}$ represents their initial mass ratio. Table 14 reveals that unlike the current situation, the secondary star had a much higher mass than the primary initially. It evolved faster and expanded beyond its Roche lobe, it began to lose mass to its companion (Yildiz & Doğan 2013). This mass transfer caused the two stars to switch roles. Later, both stars grew large enough to go beyond their Roche lobes and formed a shared envelope (Yildiz & Doğan 2013). Yildiz & Doğan (2013) also found that A-subtype CBs typically have initial secondary masses in the range of $1.7M_\odot < M_{2i} < 2.6M_\odot$, and initial primary masses in the range of $0.3M_\odot < M_{1i} < 1.5M_\odot$, assuming $\gamma = 0.664$. The initial masses derived for our targets align with these values.

To estimate the system's age, we apply the age determination model from Yıldız (2014):

$$\overline{M_2} = \frac{M_{2i} + M_L}{2}, \quad (21)$$

$$t_{\rm MS} = 10^{\left(\frac{M}{M_\odot}\right)^{-4.05}} \times \left(5.60 \times 10^{-3}\frac{M}{M_\odot} + 3.993\right)^{3.16} + 0.042, \quad (22)$$

$$t \approx t_{\rm MS}(M_{2i}) + t_{\rm MS}(M_2), \quad (23)$$

where $t_{\rm MS}$ represents the main sequence lifetime of a star. The computed results are listed in Table 14. Additionally, Yıldız (2014) established the mean age of A-subtype contact binaries as:

$$\text{age} = 4.37 \pm 1.23 \quad \text{Gyr}. \quad (24)$$

Approximately, the ages of our targets fall between 2 and 3 Gyrs, shorter than the mean age, as our targets are long-period CBs, which are more massive and evolve at a faster rate compared to other short period CBs. The notable decrease in mass ratio over a relatively short time indicates extensive mass transfer throughout their evolution.

6.4 Evolutionary Status and Stability

With the parameters displayed in Table A1, we plot systems with mass ratio lower than 0.25 and our four low-mass ratio systems in the mass–luminosity (M–L) and mass–radius (M–R) diagrams, which are shown in Fig. 7. We also plot the zero-age main sequence (ZAMS) and terminal-age main sequence (TAMS) modeled by Hurley et al. (2002) in the diagrams, respectively. All primary stars are clustered along the main sequence, positioned between ZAMS and TAMS in the diagram. In contrast, the lower-mass secondary stars appear oversized and overluminosity, placing them above the TAMS.

There exists a clear and consistent difference between the observed properties of their secondary stars and what we would expect from single stars. This key characteristic was first identified by Kuiper (1941). Two main explanations have been proposed to account for this difference. First is the possibility that the secondary star is more evolved than the primary, causing it to expand beyond its main-sequence radius, which was the assumption underlying the work of Yildiz & Doğan (2013). Second is the possibility that the secondary is not evolved, but that the transfer of energy from the primary has altered its radius. This is an idea that goes back to Kuiper (1941) and which was the assumption underlying the models of minimum mass ratio in Kobulnicky et al. (2022).

Given the same mass, long-period systems exhibit greater radii and luminosities in both components than short-period systems, implicating that the longer period primaries must be a little more evolved than their short period counterparts.

To better understand how CBs form and evolve, we calculate their the orbital angular momentum. With the binary system's total mass M_T (expressed in solar masses), period P (measured in days), and mass ratio q, the orbital angular momentum J_o of the selected contact binaries is determined. This calculation follows the equation derived by Christopoulou & Papageorgiou (2013):

$$J_o = 1.24 \times 10^{52} \times M_T^{3/5} \times P^{1/3} \times q \times (1+q)^{-2}. \quad (25)$$

We visualize the relationship between orbital angular momentum (J_o) and system's total mass in Fig. 8. This figure encompasses both detached and contact binary systems and a boundary separating them (Eker et al. 2006). The vast majority of contact binary systems are positioned below this boundary, while detached binaries are found above it. This distribution implies that the values of J_o for contact binaries are generally lower than those for detached binaries of equal mass. The transition from detached to contact binaries likely occurs through angular momentum loss mechanisms, particularly via stellar winds, contributing to shorter orbital periods (Huang 1966; Qian et al. 2007, 2015; Li et al. 2019b).

According to Darwin's instability theory (Hut 1980), the secondary component in a binary system is unable to maintain synchronous rotation with the primary due to tidal effects. As a result, the system may progress toward a merger when $\frac{J_{\rm spin}}{J_{\rm orb}} \geq \frac{1}{3}$, where $J_{\rm spin}$ represents spin angular momentum, and $J_{\rm orb}$ refers to orbital angular momentum. To study the stability of CBs, we need to calculate the ratio of spin angular momentum to orbital angular momentum (J_s/J_o), using the following equation (Yang & Qian 2015):

$$\frac{J_s}{J_o} = \frac{q}{(1+q)} \left(k_1^2 r_1^2 + k_2^2 r_2^2 q \right), \quad (26)$$

where r_1 and r_2 denote the relative radii of the primary and secondary components, while k_1^2 and k_2^2 represent the dimensionless gyration radii of the two stars.

Rasio (1995) showed that assuming $k_1^2 = 0.06$ leads to a minimum mass ratio of $q \approx 0.09$ for stability. However, the actual values of k_1^2 and k_2^2 depend on the internal structure of the primary star. For our sample, we estimate k_1 using the relations from Landin et al. (2009) for rotating and tidally distorted ZAMS stars: $k_1 = 0.5391 - 0.2504 \times M_1$ for $0.4M_\odot < M_1 < 1.4M_\odot$, and $k_1 = 0.1523 + 0.0141 \times M_1$ for $M_1 > 1.4M_\odot$. For the secondary component, we adopt $k_2^2 = 0.205$ from Arbutina (2007), as the secondary component has a very low mass and is therefore likely to be fully convective.

Using these theoretical estimates, we compute the angular momentum ratio J_s/J_o for our four targets and list in Table 14. All values are found to be below the stability limit of 1/3 (Hut 1980), confirming that these systems are currently stable.

In conclusion, photometric and spectroscopic studies of four CBs with period longer than 0.7 days, are performed. Three targets exhibit O'Connell effect. Obvious chromospheric activity is found on V0699 Cep. $O-C$ analysis shows no long-term variation in V0844 Aur and the increasing orbital periods in other three targets. Their absolute parameters, initial masses and ages are calculated. Their evolutionary status and stability are discussed. 217 CBs with both reliable radial velocity and photometric observations are collected. Differences in M–R and M–L relations between long-period and short-period systems are investigated, with 0.7 days serving as the main boundary between the two groups.

ACKNOWLEDGEMENTS

Thanks the anonymous referee very much for the constructive and insightful criticisms and suggestions to improve our manuscript. This work is supported by the National Natural Science Foundation of China (NSFC) (Nos. 12273018, 12573033), the Joint Research Fund in Astronomy (No. U1931103) under cooperative agreement between NSFC and Chinese Academy of Sciences (CAS), the Shandong Provincial Natural Science Foundation of China (Grants ZR2021QA079, ZR2025MS81), the Taishan Scholars Young Expert Program of Shandong Province, the Qilu Young Researcher Project of Shandong University, the Young Data Scientist Project of the National Astronomical Data Center, the Cultivation Project for LAMOST Scientific Payoff and Research Achievement of CAMS-CAS. The calculations in this work were carried out at Supercomputing Center of Shandong University, Weihai.

The spectral data were provided by Guoshoujing Telescope (the Large Sky Area Multi-Object Fiber Spectroscopic Telescope; LAMOST), which is a National Major Scientific Project built by the Chinese Academy of Sciences. Funding for the project has been provided by the National Development and Reform Commission. LAMOST is operated and managed by the National Astronomical Observatories, Chinese Academy of Sciences.

Based on observations obtained with the Samuel Oschin 48-inch Telescope at the Palomar Observatory as part of the Zwicky Transient Facility project. ZTF is supported by the National Science Foundation under grant No. AST-1440341 and a collaboration including Caltech, IPAC, the Weizmann Institute for Science, the Oskar Klein Center at Stockholm University, the University of Maryland, the University of Washington, Deutsches Elektronen-Synchrotron and Humboldt University, Los Alamos National Laboratories, the TANGO Consortium of Taiwan, the University of Wisconsin at Milwaukee, and Lawrence Berkeley National Laboratories. Operations are conducted by COO, IPAC, and UW.

This paper makes use of data from the DR1 of the WASP data (Butters et al. (2010)) as provided by the WASP consortium, and the computing and storage facilities at the CERIT Scientific Cloud, reg.

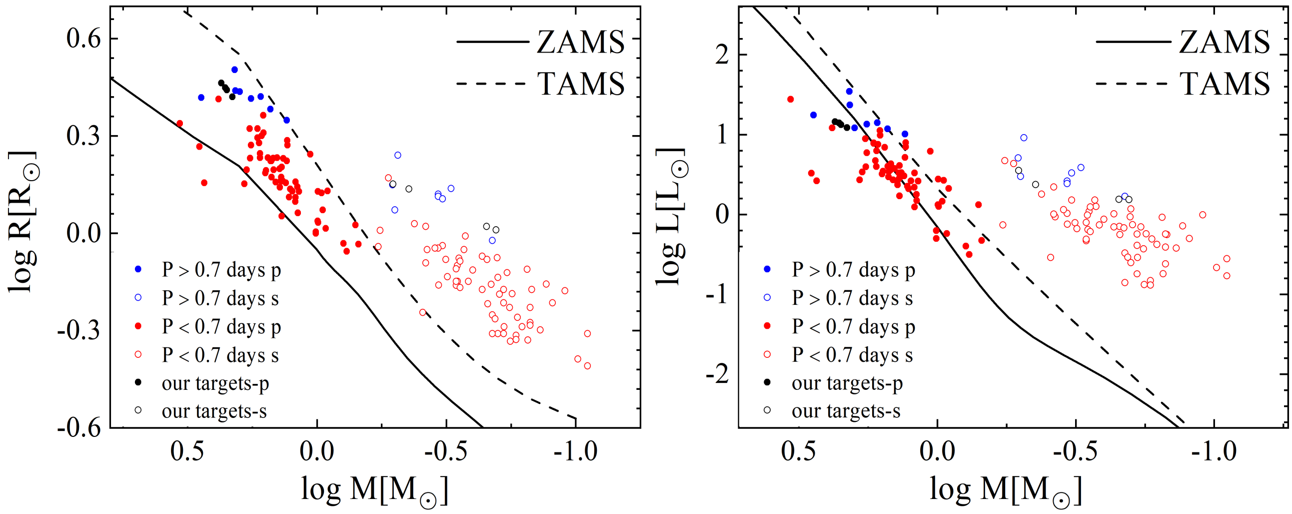

Figure 7. The *M–R* diagram and the *M–L* diagram. Solid dots represent the primary stars, while hollow circles correspond to the secondary ones. Blue represents systems with period longer than 0.7 days, red represents systems with period lower than 0.7 days, black represents our targets. The solid and dashed lines indicate the zero-age main sequence (ZAMS) and terminal-age main sequence (TAMS), respectively, as modeled by Hurley et al. (2002).

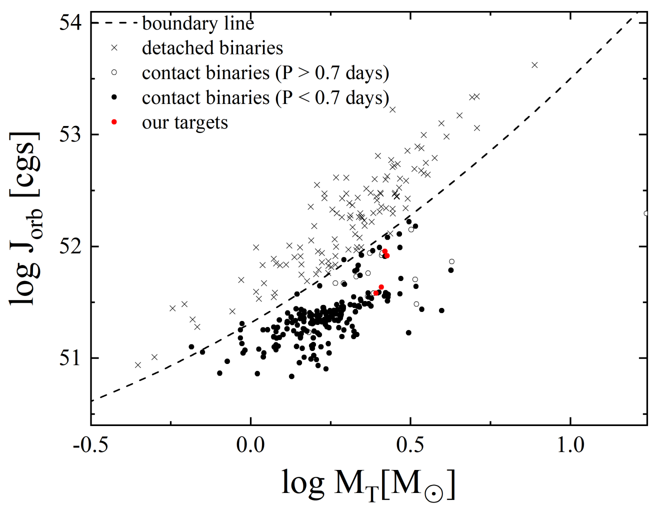

Figure 8. Relationship between orbital angular momentum and total mass for binary systems. The boundary ($J_{\rm lim}$) and the detached binaries, shown as gray crosses, are sourced from Eker et al. (2006). Hollow circles represent CBs with periods longer than 0.7 days, while solid circles signify CBs with periods lower than 0.7 days, which are displayed on Table A1. Solid red circles represent the four targets analyzed in this study.

no. CZ.1.05/3.2.00/08.0144, which is operated by Masaryk University, Czech Republic.

This work includes data collected by the TESS mission. Funding for the TESS mission is provided by NASA Science Mission Directorate. We acknowledge the TESS team for its support of this work.

We thank Las Cumbres Observatory and its staff for their continued support of ASAS-SN. ASAS-SN is funded in part by the Gordon and Betty Moore Foundation through grants GBMF5490 and GBMF10501 to the Ohio State University, and also funded in part by the Alfred P. Sloan Foundation grant G-2021-14192.

This work has made use of data from the European Space Agency (ESA) mission Gaia (https://www.cosmos.esa.int/gaia), processed by the Gaia Data Processing and Analysis Consortium (DPAC; https://www.cosmos.esa.int/web/gaia/dpac/consortium). Funding for the DPAC has been provided by national institutions, in particular the institutions participating in the Gaia Multilateral Agreement.

DATA AVAILABILITY

Here is the data link:

ASAS-SN data is available at
https://asas-sn.osu.edu/variables/lookup.
CRTS data is available at
http://crts.caltech.edu.
SuperWASP data are available at
https://wasp.cerit-sc.cz/search.
TESS data is available at
http://archive.stsci.edu/tess/bulk_downloads.html.
ZTF data is available at
https://irsa.ipac.caltech.edu/cgi-bin/ZTF.

APPENDIX A: THE PHYSICAL PARAMETERS OF 217 CBS

Table A1. The 217 CBs with Spectroscopic and Photometric Observations is listed in the appendix.

Supplementary data are available at *MNRAS* online.
Table 3. The photometric observation obtained by NEXT.
Table 10. The Eclipsing times and $O-C$ values of the four targets.

Table A1. The 217 CBs with Spectroscopic and Photometric Observations.

System	Type	P (days)	$V_{\max}$ (mag)	$q_{\rm sp}$	$q_{\rm ph}$	i (°)	a ($R_\odot$)	f (%)	T_1 (K)	T_2 (K)	M_1 ($M_\odot$)	M_2 ($M_\odot$)	R_1 ($R_\odot$)	R_2 ($R_\odot$)	L_1 ($L_\odot$)	L_2 ($L_\odot$)	$J_{\rm spin}/J_{\rm orb}$	log J_o (cgs)	Ref.
LY Aur	W	4.0020	6.68	0.528	0.528	88	36.10	–	31000	31150	25.50	14.00	16.10	12.60	213796	134896	0.1890	54.31	(1),(2)
V382 Cyg	A	1.8855	8.33	0.742	0.677	85	23.45	9	36000	34415	27.90	20.80	9.70	8.50	141905	89949	0.1665	54.38	(3)
SV Cen	W	1.6581	8.71	0.707	–	82	15.30	92	14050	23000	9.60	7.70	7.40	6.80	11700	1900	0.1159	52.29	(4),(5)
V606 Cen	A	1.4951	9.35	0.527	0.541	87	15.58	4	29200	21770	14.70	7.96	6.83	5.19	30400	5440	0.1067	53.77	(6)
TU Mus	A	1.3870	8.25	0.678	0.652	78	17.70	5	38700	33200	16.70	10.40	7.20	5.70	104712	35481	0.0973	53.91	(7)
ATO J343.6450+34.6956	A	1.1316	–	0.632	–	37	7.41	11	6862	6604	2.60	1.66	3.18	2.59	20.08	11.48	0.0580	51.86	(8)
DU Boo	A	1.0559	8.59	0.234	0.199	81	5.97	51	7850	7610	2.08	0.49	3.19	1.74	34.69	9.12	0.0712	51.92	(9),(10)
ES Lib	A	0.8830	–	0.422	–	70	5.75	15	8500	5774	2.30	0.97	2.69	1.83	33.90	3.35	0.0546	51.70	(11)
V921 Her	A	0.8774	9.44	0.226	0.227	68	5.29	23	7780	7346	2.07	0.51	2.75	1.41	23.50	5.09	0.0661	51.94	(12),(13)
II UMa	A	0.8252	8.17	0.172	0.172	78	4.91	87	6424	6418	1.99	0.34	2.73	1.32	12.14	2.62	0.0859	51.76	(14)
TY Pup	W	0.8192	8.62	0.250	0.184	84	4.65	84	6900	6915	1.65	0.30	2.64	1.37	14.11	3.86	0.0718	51.67	(15),(16)
V2388 Oph	A	0.8023	6.13	0.186	0.270	75	4.68	65	6900	6349	1.80	0.34	2.60	1.30	13.50	2.43	0.0809	51.73	(17),(18),(19),(20)
MW Pav	W	0.7950	8.51	0.220	0.222	86	4.43	69	6900	6969	1.51	0.33	2.41	1.28	11.82	3.31	0.0704	51.67	(21),(17)
V376 And	A	0.7867	7.02	0.305	0.305	63	5.32	7	9000	7080	2.44	0.74	2.60	1.51	40.00	5.00	0.0572	52.15	(22)
V1073 Cyg	A	0.7859	8.52	0.303	0.319	68	5.17	12	7300	6609	1.81	0.55	2.55	1.48	16.51	3.76	0.0548	51.94	(23),(24)
V701 Sco	W	0.7619	8.63	0.990	0.990	66	9.46	55	23440	23500	9.78	9.74	4.14	4.13	4677	4624	0.1102	52.23	(25),(26)
CX Vir	A	0.7461	–	0.343	–	83	4.58	21	6450	4694	1.73	0.59	2.24	1.39	7.78	0.84	0.0545	51.55	(27)
V144 NGC 6715	A	0.7216	19.27	0.160	–	–	3.89	20	7120	6808	1.31	0.21	2.23	0.95	10.19	1.69	0.1203	51.23	(28)
V592 Per	W	0.7157	–	0.389	–	90	4.52	54	5800	6020	1.74	0.68	2.25	1.47	9.58	2.50	0.0577	51.58	(29)
HV UMa	A	0.7108	8.69	0.190	0.184	57	5.00	77	7300	7000	2.80	0.50	2.62	1.18	17.50	3.00	0.0768	51.48	(30)
FN Cam	W	0.6771	8.58	0.222	0.222	71	4.64	88	6700	6848	2.40	0.53	2.59	1.48	12.11	4.32	0.0848	51.99	(31),(32)
FT UMa	A	0.6547	–	0.984	–	63	4.55	15	7178	7003	1.49	1.46	1.79	1.78	7.68	6.86	0.0716	51.71	(33)
AG Vir	A	0.6427	8.50	0.341	0.382	84	4.48	17	8150	6915	2.18	0.74	2.19	1.36	19.00	3.85	0.0566	52.11	(10),(23)
FP Boo	A	0.6405	10.14	0.096	0.100	69	3.78	39	6980	6456	1.61	0.15	2.31	0.77	11.19	0.92	0.1400	51.36	(34),(13)
V868 Mon	A	0.6377	8.90	0.373	0.373	84	4.63	46	7400	6484	2.39	0.89	2.33	1.56	14.70	3.89	0.0642	52.18	(35),(36)
V407 Peg	A	0.6369	9.28	0.256	0.256	88	4.02	61	6980	6484	1.72	0.43	2.15	1.21	9.80	2.33	0.0671	51.79	(37),(38),(39)
CT Eri	A	0.6342	–	0.300	–	69	3.99	69	6881	5086	1.62	0.49	2.09	1.30	8.80	1.01	0.0650	51.47	(40)
V535 Ara	A	0.6293	7.17	0.302	0.361	80	4.20	22	8200	8129	1.94	0.59	2.09	1.23	18.00	6.00	0.0573	51.99	(41)
SZ Hor	A	0.6251	11.01	0.470	0.470	80	4.28	14	6881	5183	1.82	0.86	1.95	1.38	7.61	1.23	0.0519	52.08	(15),(40)
V0663 Peg	A	0.6245	–	0.220	–	89	3.52	29	6972	6183	1.30	0.27	1.93	0.98	7.91	1.26	0.0948	51.31	(8)
UZ Leo	W	0.6180	9.61	0.306	0.233	90	4.21	75	6980	7094	2.01	0.62	2.23	1.40	10.60	3.68	0.0686	51.91	(38)
BX And	A	0.6101	9.05	0.445	0.623	76	4.42	5	6650	4758	2.15	0.98	2.01	1.40	7.08	0.90	0.0521	52.22	(42),(27)
V0751 Peg	A	0.6076	–	0.190	–	70	3.26	22	6884	6193	1.06	0.20	1.75	0.84	6.20	0.94	0.1510	51.21	(8)
RR Cen	A	0.6057	7.27	0.210	0.205	81	3.92	43	6912	6891	1.82	0.38	2.10	1.05	8.89	2.20	0.0702	51.74	(43),(44)
V402 Aur	A	0.6035	8.84	0.200	0.201	53	3.77	3	6775	6700	1.64	0.33	2.00	0.92	7.54	1.52	0.0665	51.66	(43),(45)
ASASSN-V J230252.69+342300.6	W	0.6010	–	0.373	–	55	3.69	54	6689	6754	1.35	0.51	1.85	1.24	6.18	2.85	0.0690	51.48	(8)
HI Dra	A	0.5974	9.02	0.250	0.250	55	3.80	23	7000	6550	1.70	0.42	1.97	1.07	7.87	1.80	0.0621	51.78	(46),(47),(48)
AQ Tuc	W	0.5949	9.91	0.354	0.270	76	4.11	37	6900	7048	1.93	0.69	2.05	1.32	8.95	3.47	0.0593	51.55	(49),(50)
V351 Peg	A	0.5933	–	0.360	–	63	3.87	21	7580	7559	1.63	0.59	1.87	1.19	9.95	3.99	0.0537	51.51	(51)
V2150 Cyg	A	0.5919	–	0.802	–	43	4.80	23	8000	7920	2.35	1.89	1.98	1.79	14.45	11.27	0.0643	51.79	(52)
eps CrA	A	0.5914	5.61	0.128	–	74	3.69	27	6678	6341	1.70	0.23	2.10	0.85	7.75	1.02	0.1010	51.19	(44),(53)
ASAS 185843-3706.4	A	0.5914	4.74	0.137	0.128	1	3.69	25	6678	6341	1.70	0.23	2.10	0.85	7.75	1.02	0.0959	51.50	(44),(53)
V401 Cyg	A	0.5827	10.84	0.290	0.300	77	3.80	46	6700	6650	1.68	0.49	1.91	1.17	6.57	2.39	0.0599	51.83	(17),(54)
BX Dra	A	0.5790	–	0.288	–	82	4.06	60	6980	6758	2.08	0.60	2.13	1.28	9.66	3.05	0.0669	51.51	(55)
V357 Peg	A	0.5785	9.01	0.401	0.401	73	3.92	10	7000	6438	1.72	0.69	2.12	1.25	9.67	2.41	0.0611	51.96	(37),(56)
XX Sex	A	0.5401	9.32	0.100	0.100	75	3.15	48	6881	6378	1.30	0.13	1.87	0.70	7.02	0.72	0.1877	51.18	(40),(57)
BO CVn	W	0.5175	–	0.340	–	89	3.14	83	6980	7191	1.16	0.39	1.62	1.00	5.53	2.38	0.0927	51.39	(58)
V0747 Peg	A	0.5143	–	0.066	–	65	3.24	79	7162	7070	1.61	0.11	2.04	0.66	9.83	0.99	0.2055	50.90	(8)
BV Eri	A	0.5077	8.13	0.300	0.253	75	2.99	32	6881	5737	1.07	0.32	1.51	0.89	4.56	0.77	0.1049	51.44	(15),(40)
OO Aql	A	0.5068	9.50	0.846	0.843	88	3.35	31	6100	5926	1.06	0.90	1.41	1.31	2.45	1.89	0.0868	51.88	(59),(57)
DN Cam	W	0.4983	–	0.442	–	73	3.67	49	6530	6700	1.85	0.82	1.78	1.22	5.14	2.71	0.0572	51.58	(60)
AH Aur	W	0.4941	–	0.165	–	76	3.29	75	6200	6418	1.67	0.28	1.90	0.84	4.73	1.09	0.0881	51.25	(61)
V1003 Her	W	0.4933	9.81	0.373	–	38	3.74	36	6335	6885	1.96	0.73	1.83	1.20	4.85	2.88	0.0575	51.55	(62)
Y Sex	A	0.4877	–	0.195	–	79	2.85	60	6650	6448	1.47	0.29	1.57	0.80	4.31	0.98	0.0746	51.27	(40)
TT Cet	A	0.4860	–	0.390	–	82	3.73	8	6765	5230	2.11	0.82	1.73	1.16	5.61	0.89	0.0528	51.57	(40)
EL Aqr	A	0.4814	10.35	0.203	–	71	3.25	44	6881	6137	1.66	0.34	1.76	0.90	6.25	1.03	0.0726	51.32	(63)
NN Vir	W	0.4807	–	0.491	–	66	3.57	55	7148	7201	1.77	0.87	1.72	1.29	6.94	4.03	0.0623	51.58	(40)
VW LMi	A	0.4776	–	0.423	–	78	3.43	50	6440	6180	1.68	0.71	1.69	1.18	4.41	1.82	0.0598	51.53	(9)
AQ Psc	A	0.4756	–	0.226	–	69	3.25	30	6250	6024	1.66	0.38	1.71	0.89	3.99	0.94	0.0650	51.35	(40)
TYC 5532-1333-1	A	0.4745	11.09	0.240	–	85	2.98	34	6380	6328	1.51	0.35	1.67	0.90	4.02	1.15	0.0721	51.34	(64)
V728 Her	W	0.4713	–	0.178	–	69	3.22	81	6600	6743	1.80	0.28	1.87	0.82	5.90	1.24	0.0861	51.28	(65)
DK Cyg	A	0.4707	–	0.307	–	83	3.40	45	7500	7011	1.82	0.56	1.74	1.05	8.50	2.40	0.0609	51.46	(66)
FT Lup	A	0.4701	–	0.440	–	89	3.54	13	6700	4651	1.87	0.82	1.64	1.13	4.86	0.54	0.0526	51.57	(27)
AA UMa	W	0.4681	–	0.551	–	80	3.44	14	5920	5964	1.61	0.89	1.53	1.17	2.57	1.55	0.0538	51.58	(67)
CN And	A	0.4628	–	0.387	–	68	3.14	0	6350	5732	1.40	0.55	1.45	0.94	3.41	0.93	0.0481	51.46	(68)
KIC 9832227	W	0.4580	–	0.228	–	53	2.99	43	5800	5920	1.40	0.32	1.58	0.83	2.61	0.79	0.0735	51.30	(69)
CN Hyi	A	0.4561	–	0.184	–	64	2.93	43	6500	6360	1.37	0.25	1.60	0.77	4.10	0.87	0.0905	51.22	(70)
V502 Oph	W	0.4534	–	0.335	–	76	3.04	35	5900	6140	1.37	0.46	1.51	0.94	2.49	1.13	0.0640	51.41	(71)
EZ Hya	W	0.4497	–	0.257	–	83	2.98	34	5721	6100	1.37	0.35	1.54	0.85	2.28	0.90	0.0712	51.33	(72)
V445 Cep	A	0.4488	6.84	0.167	–	20	3.90	52	9015	8460	3.39	0.57	2.18	1.02	27.70	4.71	0.1039	51.42	(73)
DN Boo	A	0.4476	–	0.103	–	60	2.86	64	6095	6071	1.43	0.15	1.71	0.67	3.75	0.56	0.1260	51.02	(74)
TV Mus	A	0.4457	–	0.166	–	77	2.98	74	5980	5808	1.35	0.22	1.70	0.83	3.33	0.71	0.1110	51.18	(75)
UX Eri	W	0.4453	–	0.373	–	76	3.07	20	6006	6093	1.42	0.53	1.47	0.95	2.52	1.10	0.0518	51.45	(40)
VY Sex	W	0.4434	–	0.313	–	66	3.00	25	5877	5960	1.41	0.44	1.48	0.88	2.35	0.88	0.0535	51.39	(40)
V972 Her	W	0.4431	6.65	0.167	–	40	2.49	1	6099	6522	0.91	0.15	1.35	0.59	2.11	0.57	0.2124	51.08	(76),(17)
DY Cet	A	0.4408	–	0.356	–	82	3.05	26	6650	6611	1.44	0.51	1.48	0.94	3.84	1.51	0.0531	51.44	(40)
V776 Cas	A	0.4404	–	0.130	–	55	2.94	65	7000	6920	1.55	0.20	1.71	0.73	6.93	1.17	0.1038	51.13	(77)
KIC 10618253	A	0.4374	–	0.125	–	82	2.87	93	6118	5970	1.48	0.18	1.70	0.76	3.64	0.70	0.1110	51.10	(78)
ASASSN-V J231002.29+342823.4	A	0.4340	–	0.365	–	81	5.93	9	6897	5027	1.33	0.85	2.58	1.88	13.54	2.03	0.0584	51.47	(8)
HI Pup	A	0.4326	10.54	0.206	–	82	2.72	20	6500	6377	1.21	0.23	1.44	0.67	3.30	0.70	0.1065	51.22	(79)
V1363 Ori	A	0.4319	10.30	0.205	–	57	2.80	73	6750	6789	1.31	0.27	1.67	0.89	5.19	1.51	0.1181	51.24	(80),(81),(82)
AP Leo	W	0.4304	–	0.297	–	78	2.97	14	6150	6250	1.46	0.43	1.48	0.82	2.80	0.91	0.0525	51.38	(52)
V2610 Oph	A	0.4265	9.20	0.291	0.550	72	2.87	0	5940	6157	1.25	0.36	1.41	0.80	2.25	0.84	0.0753	51.34	(83),(84),(85)
V2377 Oph	W	0.4254	–	0.395	–	44	2.70	6	5418	5940	1.04	0.41	1.25	0.82	1.21	0.74	0.0858	51.37	(40)
EF Dra	A	0.4240	–	0.160	–	78	3.05	47	6250	6186	1.82	0.29	1.70	0.78	3.96	0.79	0.0872	51.24	(86)
ER Ori	W	0.4234	9.28	0.656	0.641	86	3.23	15	6200	6267	1.54	0.98	1.39	1.14	1.93	1.80	0.0564	51.59	(46),(87),(88)
TYC 2675-663-1	A	0.4224	–	0.810	–	65	3.14	14	6480	5534	1.29	1.04	1.22	1.11	2.40	1.04	0.0621	51.58	(89)
AK Her	A	0.4215	–	0.277	–	82	2.73	33	6500	6180	1.20	0.34	1.40	0.80	3.02	0.82	0.0915	51.31	(47)
V899 Her	A	0.4212	–	0.566	–	69	3.51	24	5700	5677	2.10	1.19	1.57	1.22	2.32	1.40	0.0571	51.64	(90)
EF Boo	W	0.4205	–	0.534	–	76	3.14	25	6425	6450	1.55	0.79	1.43	1.06	3.08	1.73	0.0543	51.55	(61)
GSC 02757-00769	A	0.4192	–	0.214	–	62	2.51	41	6426	6292	0.99	0.21	1.35	0.70	2.77	0.68	0.1568	51.18	(8)
V404 Peg	A	0.4192	–	0.243	–	62	2.67	32	6340	6154	1.18	0.29	1.35	0.71	2.62	0.65	0.0958	51.26	(91)
V842 Her	W	0.4190	–	0.259	–	78	2.88	25	5723	6020	1.45	0.38	1.47	0.81	2.08	0.77	0.0582	51.34	(92)
BL Eri	A	0.4169	11.50	0.540	0.546	90	2.30	16	5980	5603	0.61	0.33	1.18	0.53	1.02	0.78	0.1288	51.31	(93),(94)
RZ Tau	A	0.4157	–	0.376	–	84	3.11	56	7300	7200	1.70	0.64	1.56	1.04	6.19	2.60	0.0602	51.49	(95)
V2357 Oph	W	0.4156	10.51	0.231	–	47	2.67	23	5640	5780	1.19	0.29	1.39	0.69	1.78	0.47	0.1008	51.25	(12),(96)
UV Lyn	W	0.4150	–	0.372	–	68	2.87	19	5770	6000	1.34	0.50	1.38	0.86	1.86	0.84	0.0598	51.42	(29)
V1918 Cyg	A	0.4132	–	0.278	–	81	2.77	31	7300	6784	1.30	0.36	1.36	0.76	4.72	1.10	0.0704	51.33	(97)
QX And	A	0.4122	–	0.306	–	55	2.89	36	6440	6420	1.47	0.45	1.46	0.88	3.16	1.14	0.0574	51.39	(98)
GSC 03950-00707	A	0.4120	13.36	0.205	–	–	3.52	12	5729	5623	2.85	0.58	1.85	0.91	3.29	0.74	0.0767	51.44	(99),(100)
V566 Oph	A	0.4096	–	0.250	–	80	2.86	34	6456	6433	1.50	0.38	1.49	0.81	3.43	1.01	0.0614	51.33	(76)
V839 Oph	W	0.4090	–	0.305	–	80	2.98	60	6381	6424	1.63	0.50	1.55	0.96	3.55	1.39	0.0627	51.41	(40)
EX Leo	A	0.4086	–	0.200	–	61	2.86	37	6340	6110	1.57	0.31	1.56	0.73	3.47	0.66	0.0704	51.27	(101)
KR Com	A	0.4080	7.20	0.091	–	52	2.36	–	5549	6072	0.96	0.09	1.33	0.49	1.46	0.28	0.3494	50.86	(17),(102)
AH Vir	W	0.4075	–	0.303	–	85	2.80	23	5300	5671	1.36	0.41	1.40	0.83	1.86	0.63	0.0656	51.36	(103)
SS Ari	W	0.4060	10.37	0.295	–	77	2.78	9	5860	6123	1.34	0.41	1.37	0.80	1.83	0.71	0.0662	51.35	(104)
BH Cas	W	0.4059	–	0.475	–	71	2.59	16	4874	5163	0.96	0.46	1.19	0.85	0.70	0.46	0.0909	51.39	(105)
TMTS J01322049+5512196	W	0.4009	–	0.676	–	84	2.98	13	6165	6244	1.33	0.90	1.27	1.07	2.10	1.56	0.0884	51.92	(106)
V1123 Tau	W	0.3999	–	0.279	–	74	2.68	30	5821	5920	1.27	0.35	1.36	0.78	1.91	0.66	0.0799	51.32	(56)
V870 Ara	W	0.3997	–	0.082	–	70	2.59	98	5860	6210	1.50	0.12	1.67	0.61	2.96	0.50	0.1774	50.93	(107)
AR CrB	W	0.3974	10.83	0.836	–	76	2.91	5	5640	5690	1.14	0.96	1.15	1.06	1.20	1.06	0.0720	51.55	(108)

Table A1. The 217 CBs with Spectroscopic and Photometric Observations. (Continued).

System	Type	P (days)	$V_{\max}$ (mag)	$q_{\rm sp}$	$q_{\rm ph}$	i (°)	a ($R_\odot$)	f (%)	T_1 (K)	T_2 (K)	M_1 ($M_\odot$)	M_2 ($M_\odot$)	R_1 ($R_\odot$)	R_2 ($R_\odot$)	L_1 ($L_\odot$)	L_2 ($L_\odot$)	$J_{\rm spin}/J_{\rm orb}$	$\log J_o$ (cgs)	Ref.
FI Boo	W	0.3900	–	0.373	–	38	2.55	49	5420	5746	1.07	0.40	1.28	0.85	1.27	0.71	0.0995	51.35	(109)
TYC 1174-344-1	A	0.3887	11.03	0.187	–	88	2.64	52	6500	6357	1.38	0.26	1.45	0.71	3.31	0.74	0.0893	51.21	(110)
AU Ser	A	0.3865	–	0.692	–	82	2.52	4	5140	4986	0.85	0.59	1.04	0.88	0.68	0.43	0.0866	51.43	(111)
BI CVn	W	0.3842	–	0.413	–	71	2.92	31	6093	6170	1.61	0.66	1.40	0.96	2.44	1.19	0.0554	51.48	(112)
V546 And	W	0.3830	–	0.254	–	86	2.46	30	6240	6517	1.08	0.28	1.23	0.66	2.05	0.71	0.1071	51.24	(113)
TX Cnc	W	0.3829	–	0.455	–	62	2.76	17	6121	6250	1.32	0.60	1.27	0.89	2.03	1.09	0.0604	51.46	(40)
HN UMa	A	0.3826	–	0.145	–	48	2.84	29	6252	5946	1.91	0.19	1.42	0.61	2.72	0.41	0.0742	51.19	(114)
LO And	W	0.3804	–	0.305	–	80	2.74	40	6650	6690	1.47	0.45	1.40	0.84	3.44	1.27	0.0586	51.38	(115)
EE Cet	W	0.3799	8.76	0.315	–	64	2.69	22	6095	6314	1.37	0.43	1.35	0.82	2.25	0.96	0.0655	51.37	(40)
AD Phe	A	0.3799	–	0.376	–	76	2.46	16	6155	5835	1.00	0.38	1.17	0.76	1.76	0.60	0.0954	51.34	(116)
HX UMa	A	0.3792	8.74	0.291	–	49	2.72	59	6650	6601	1.44	0.32	1.61	1.15	4.54	2.25	0.0936	51.34	(117)
USNO-B1.0 1452-0049820	A	0.3782	14.67	0.111	–	–	2.50	5	6400	6300	1.32	0.15	1.43	0.53	3.03	0.39	0.1527	51.01	(118)
DX Tuc	A	0.3771	–	0.290	–	62	2.53	20	6250	6182	1.00	0.30	1.20	0.71	1.97	0.66	0.1042	51.26	(107)
NSVS 5029961	A	0.3767	11.54	0.152	–	–	2.84	19	6260	6192	1.87	0.28	1.57	0.68	3.40	0.61	0.0875	51.21	(119)
YY CrB	W	0.3766	–	0.232	–	80	2.64	23	6100	6499	1.39	0.34	1.39	0.69	2.35	0.76	0.0705	51.28	(61)
1SWASP J034501.24+493659.9	W	0.3765	–	0.421	–	60	2.14	25	6494	6514	0.65	0.28	1.01	0.69	1.63	0.78	0.1375	51.25	(120)
HH UMa	A	0.3755	–	0.295	–	52	2.58	41	6550	6297	1.25	0.37	1.32	0.78	3.03	0.86	0.0830	51.32	(121)
V2612 Oph	W	0.3753	–	0.286	–	67	2.59	22	6250	6280	1.30	0.37	1.30	0.75	2.23	0.75	0.0738	51.32	(47)
RT LMi	W	0.3749	–	0.382	–	83	2.65	28	6200	6350	1.31	0.48	1.29	0.81	2.18	0.93	0.0647	51.40	(101)
U Peg	W	0.3748	–	0.331	–	76	2.53	15	5600	5800	1.17	0.39	1.23	0.75	1.29	0.55	0.0814	51.34	(122)
HV Aqr	W	0.3745	–	0.145	–	79	2.53	57	6460	6669	1.36	0.20	1.45	0.65	3.27	0.74	0.1184	51.11	(123)
V0593 And	A	0.3722	–	0.397	–	67	2.38	9	5874	5524	0.93	0.37	1.11	0.73	1.04	0.58	0.0995	51.33	(8)
V417 Aql	W	0.3703	–	0.362	–	82	2.70	23	6252	6381	1.41	0.51	1.30	0.83	2.33	1.02	0.0524	51.41	(40)
V752 Cen	W	0.3702	9.10	0.311	0.299	82	2.59	6	5955	6221	1.30	0.40	1.28	0.75	1.85	0.76	0.0695	51.35	(124),(125)
BD +42 2782	W	0.3702	–	0.482	–	74	2.75	37	5850	6039	1.38	0.67	1.29	0.95	1.75	1.05	0.0616	51.48	(126)
V410 Aur	A	0.3664	–	0.144	–	82	2.44	32	5950	5898	1.27	0.18	1.37	0.59	2.10	0.37	0.1362	51.09	(127)
DZ Psc	A	0.3661	–	0.136	–	78	2.49	95	6210	6124	1.37	0.19	1.46	0.67	2.85	0.57	0.1272	51.09	(128)
AM Leo	W	0.3658	–	0.440	–	89	2.60	22	5942	6273	1.23	0.54	1.22	0.85	1.67	1.00	0.0700	51.42	(129)
LS Del	W	0.3638	–	0.375	–	45	2.57	20	6192	6250	1.25	0.47	1.23	0.79	1.99	0.93	0.0693	51.39	(40)
AE Phe	W	0.3624	7.56	0.394	0.392	86	2.53	15	6083	6310	1.18	0.47	1.19	0.78	1.74	0.86	0.0736	51.38	(130),(131)
BB Peg	W	0.3615	–	0.318	–	84	2.52	47	6121	6355	1.24	0.41	1.25	0.79	1.97	0.91	0.0798	51.34	(132)
VZ Lib	W	0.3583	10.13	0.237	0.236	80	2.43	52	5387	5770	1.21	0.29	1.29	0.71	1.24	0.49	0.1037	51.24	(32),(107),(133)
V829 Her	W	0.3582	–	0.435	–	57	2.61	20	6194	6300	1.30	0.57	1.22	0.84	1.95	0.99	0.0634	51.43	(134)
QW Gem	W	0.3581	–	0.334	–	80	2.56	15	6200	6370	1.30	0.44	1.24	0.76	1.98	0.79	0.0668	51.36	(135)
CK Boo	A	0.3552	–	0.111	–	61	2.55	95	6250	6234	1.58	0.18	1.53	0.65	3.21	0.57	0.1251	51.04	(40)
TY UMa	W	0.3545	–	0.396	–	85	2.74	13	6229	6250	1.57	0.62	1.29	0.85	0.99	0.63	0.0513	51.46	(136)
TMTS J06380824+4412135	W	0.3544	–	0.730	–	72	2.35	15	5263	5518	0.81	0.59	0.98	0.86	0.67	0.61	0.1106	51.57	(106)
AC Boo	W	0.3524	–	0.299	–	86	2.43	5	6241	6250	1.20	0.36	1.19	0.69	1.94	0.65	0.0808	51.31	(137)
NSVS 4161544	W	0.3517	–	0.296	–	65	2.60	10	5726	6016	1.47	0.44	1.29	0.74	1.51	0.65	0.0537	51.36	(120)
BV Dra	W	0.3501	–	0.411	–	76	1.65	22	6245	6345	1.04	0.43	1.12	0.76	1.71	0.84	0.1833	51.36	(138)
NSVS 2256852	A	0.3489	12.93	0.162	–	–	2.16	17	6804	5606	0.95	0.15	1.18	0.52	2.67	0.24	0.2080	51.04	(99),(139)
GR Vir	W	0.3470	–	0.106	–	82	2.40	93	6150	6554	1.38	0.17	1.49	0.55	2.81	0.49	0.1638	50.99	(61)
ET Leo	W	0.3465	–	0.342	–	37	2.67	55	5112	5500	1.59	0.54	1.36	0.84	1.12	0.56	0.0579	51.42	(13)
V781 Tau	W	0.3449	–	0.453	–	66	2.72	24	5575	6000	1.57	0.71	1.26	0.89	1.38	0.92	0.0528	51.49	(140)
V508 Oph	A	0.3448	10.06	0.530	0.552	84	2.36	15	5980	5878	1.01	0.52	1.06	0.80	1.29	0.69	0.0837	51.40	(141),(142)
V757 Cen	W	0.3432	–	0.671	–	69	2.35	14	5927	6000	0.88	0.59	0.97	0.80	1.02	0.73	0.0831	51.42	(143)
VW Boo	W	0.3423	–	0.428	–	74	2.38	16	5198	5560	1.08	0.46	1.11	0.76	0.81	0.49	0.0811	51.37	(144)
EQ Tau	A	0.3413	–	0.439	–	85	2.49	9	5800	5730	1.23	0.54	1.14	0.79	1.33	0.61	0.0663	51.41	(145)
GM Dra	W	0.3387	8.80	0.210	–	63	2.31	40	6306	6450	1.21	0.22	1.25	0.61	2.19	0.56	0.1113	51.19	(61)
RZ Com	W	0.3385	–	0.460	–	87	2.49	17	5257	5420	1.25	0.57	1.15	0.82	1.63	0.93	0.0671	51.43	(146)
V0579 And	A	0.3381	–	0.254	–	66	2.16	49	5759	5460	0.94	0.24	1.13	0.64	1.01	0.40	0.1466	51.19	(8)
TMTS J22364231+3041479	W	0.3357	–	0.518	–	80	2.40	13	5503	5754	1.08	0.56	1.08	0.80	0.96	0.63	0.1279	51.65	(106)
W UMa	W	0.3336	7.75	0.490	–	86	2.41	10	5800	6194	1.15	0.54	1.13	0.81	1.27	0.86	0.0767	51.42	(147)
AB And	W	0.3319	–	0.560	–	83	2.37	25	5020	5450	1.03	0.58	1.15	0.82	0.77	0.53	0.0903	51.42	(148)
AO Cam	W	0.3299	–	0.435	–	76	2.35	17	5590	6200	1.12	0.49	1.09	0.73	1.05	0.71	0.0761	51.38	(60)
FG Hya	W	0.3278	–	0.104	–	83	2.34	70	6200	6519	1.45	0.16	1.44	0.52	2.70	0.42	0.1303	50.99	(101)
V505 Lac	W	0.3270	10.00	0.395	–	57	2.21	13	5166	5600	0.97	0.38	1.04	0.69	0.68	0.41	0.0965	51.32	(149)
YY Eri	W	0.3216	8.10	0.454	–	82	2.55	5	5349	5600	1.54	0.62	1.20	0.77	1.07	0.53	0.0487	51.46	(150)
SW Lac	W	0.3207	–	0.787	–	80	2.57	35	5515	5800	1.24	0.96	1.09	0.98	0.97	0.95	0.0744	51.53	(61)
HH Boo	A	0.3187	–	0.587	–	69	2.34	11	5680	5386	1.07	0.63	1.00	0.78	0.75	0.57	0.0725	51.43	(151)
BO Ari	A	0.3182	–	0.190	–	82	2.08	49	5940	5908	1.00	0.19	1.09	0.52	1.33	0.29	0.1602	51.10	(152)
NSVS 1917038	A	0.3181	13.28	0.146	–	–	–	4	5074	4869	–	–	–	–	–	–	–	–	(153)
NSVS 254037	W	0.3175	10.56	0.413	–	67	2.30	10	5585	5800	1.15	0.47	1.07	0.72	1.00	0.53	0.0751	51.37	(149)
TW Cet	W	0.3169	–	0.750	–	81	2.33	6	5753	5865	0.96	0.72	0.95	0.83	0.89	0.73	0.0801	51.45	(40)
SX Crv	A	0.3166	–	0.079	–	61	2.16	27	6340	6160	1.25	0.10	1.35	0.41	2.63	0.22	0.2827	50.84	(43)
TMTS J10421306+3849120	W	0.3160	–	0.350	–	62	2.21	26	5313	5652	0.97	0.34	1.05	0.66	0.79	0.40	0.2033	51.40	(106)
V1191 Cyg	W	0.3134	–	0.107	–	81	2.18	58	6215	6378	1.28	0.14	1.29	0.50	2.25	0.38	0.1840	50.96	(154)
PY Vir	A	0.3112	–	0.773	–	70	2.30	0	4830	4702	0.95	0.74	0.92	0.82	0.42	0.29	0.0796	51.45	(155)
FU Dra	W	0.3067	10.68	0.251	–	80	2.14	27	5823	6100	1.12	0.28	1.10	0.60	1.26	0.45	0.1094	51.21	(156),(157)
V1128 Tau	W	0.3054	–	0.534	–	86	2.27	13	6200	6400	1.10	0.58	1.01	0.76	1.29	0.84	0.0748	51.41	(47)
GZ And	A	0.3050	–	0.532	–	87	2.28	12	5810	5500	1.12	0.59	1.01	0.74	1.03	0.45	0.0710	51.42	(60)
TMTS J13001158+3023102	W	0.3020	–	0.222	–	79	1.79	6	4970	5502	0.69	0.15	0.93	0.47	0.47	0.18	0.3869	50.97	(106)
BN Ari	W	0.2994	–	0.392	–	84	2.14	13	5170	5278	1.05	0.41	0.99	0.65	0.69	0.27	0.0832	51.32	(158)
TZ Boo	W	0.2972	–	0.207	–	85	1.99	53	5890	5926	0.99	0.21	1.08	0.56	1.26	0.33	0.1652	51.12	(159)
OU Ser	A	0.2968	–	0.173	–	50	2.09	67	5940	5759	1.19	0.21	1.16	0.54	1.49	0.29	0.1370	51.10	(40)
TMTS J07592990+4019452	W	0.2960	–	0.183	–	78	1.93	15	4947	5144	0.93	0.17	1.03	0.48	0.58	0.15	0.4731	51.01	(106)
UW CVn	W	0.2925	14.85	0.245	–	–	–	20	5500	5889	–	–	–	–	–	–	–	–	(160),(161)
BW Dra	W	0.2922	–	0.280	–	74	1.36	14	5980	6164	0.92	0.26	0.98	0.55	1.10	0.39	0.2676	51.19	(138)
RW Dor	W	0.2855	–	0.630	–	77	2.03	3	5287	5560	0.82	0.52	0.88	0.70	0.53	0.42	0.0944	51.36	(162)
ASAS J102556+2049.3	A	0.2850	10.66	0.131	–	–	1.69	24	6010	5941	0.71	0.09	1.06	0.39	1.32	0.17	0.4558	50.86	(99)
XY Leo	W	0.2841	–	0.729	–	69	2.07	21	4742	5150	0.85	0.62	0.88	0.76	0.35	0.37	0.0930	51.40	(40)
GW Cnc	W	0.2814	–	0.265	–	83	1.94	22	5649	5790	0.97	0.26	0.96	0.53	0.84	0.28	0.1225	51.18	(163)
BX Peg	W	0.2804	–	0.376	–	87	2.02	18	5300	5887	1.02	0.38	0.97	0.62	0.66	0.32	0.0945	51.29	(164)
TMTS J09135321+4354212	W	0.2787	–	0.935	–	67	1.60	3	5142	5523	0.42	0.29	0.68	0.57	0.29	0.27	0.1313	51.05	(106)
VW Cep	W	0.2783	–	0.302	–	63	2.03	0	5050	5342	1.13	0.34	0.99	0.57	0.57	0.24	0.0883	51.26	(165)
PY Boo	W	0.2781	12.40	0.222	–	–	1.77	18	4770	5080	0.79	0.17	0.93	0.47	0.40	0.13	0.1947	51.07	(99)
BD+07 3142	W	0.2752	9.89	0.662	–	72	1.91	10	4640	4900	0.74	0.49	0.81	0.67	0.26	0.23	0.0984	51.34	(98),(37)
V1167 Her	W	0.2752	–	0.662	–	72	1.91	9	4640	4900	0.74	0.49	0.81	0.67	0.27	0.23	0.0984	51.34	(98)
V345 Gem	A	0.2748	8.03	0.171	–	73	2.07	11	6200	5840	1.37	0.20	1.13	0.49	1.71	0.25	0.0919	51.12	(166),(167)
NSVS 7328383	A	0.2721	13.01	0.205	–	–	1.89	17	5146	5056	1.01	0.21	1.00	0.49	0.63	0.14	0.1514	51.11	(168)
i Boo	W	0.2678	5.80	0.487	0.559	73	1.91	0	5300	5035	0.83	0.47	0.80	0.60	0.44	0.21	0.0889	51.31	(169),(170)
44 Boo	A	0.2678	–	0.559	–	73	2.02	0	5300	5035	0.98	0.55	0.87	0.66	0.51	0.24	0.0791	51.38	(169)
GV Leo	W	0.2667	11.58	0.188	–	–	1.85	18	4850	5344	1.01	0.19	1.01	0.49	0.50	0.18	0.1714	51.07	(171),(172)
VZ Psc	A	0.2613	10.20	0.800	–	56	1.90	96	4908	4011	0.74	0.60	0.80	0.65	0.33	0.10	0.0931	51.37	(173),(174)
TMTS J00474579+3931052	W	0.2611	–	0.233	–	62	1.69	24	4610	5113	0.77	0.18	0.88	0.46	0.32	0.13	0.3695	51.05	(106)
TMTS J14020545+3402396	W	0.2608	–	0.457	–	88	1.68	13	4408	4544	0.64	0.29	0.77	0.54	0.20	0.11	0.1766	51.18	(106)
1SWASP J150822.80-054236.9	A	0.2601	–	0.510	–	90	2.01	16	4500	4500	1.07	0.55	0.90	0.68	0.30	0.17	0.0791	51.37	(175)
V0568 Peg	A	0.2471	–	0.449	–	70	1.73	11	4648	4429	0.78	0.35	0.79	0.55	0.22	0.13	0.1109	51.25	(8)
TMTS J03050520+2934439	W	0.2470	–	0.351	–	71	1.62	26	4641	4822	0.70	0.24	0.79	0.50	0.26	0.12	0.2379	51.13	(106)
ASAS J142124+1813.1	A	0.2427	12.88	0.144	–	–	2.40	23	6160	5630	2.73	0.39	1.43	0.57	2.64	0.29	0.1159	51.23	(99),(176)
RW Com	W	0.2373	–	0.471	–	72	1.72	18	4517	4830	0.83	0.39	0.79	0.56	0.23	0.15	0.1040	51.27	(40)
V523 Cas	W	0.2337	10.64	0.516	0.510	85	1.69	29	4762	5104	0.78	0.40	0.78	0.58	0.27	0.20	0.1106	51.28	(12),(177),(178)
1SWASP J093010.78+533859.5	A	0.2277	–	0.397	–	86	1.67	17	4700	4700	0.86	0.34	0.79	0.52	0.27	0.12	0.1106	51.24	(179)
1SWASP J160156.04+202821.6	A	0.2265	–	0.670	–	80	1.76	13	4500	4500	0.86	0.57	0.75	0.63	0.21	0.15	0.0913	51.35	(175)
CC Com	W	0.2207	–	0.526	–	90	1.58	16	4200	4300	0.72	0.38	0.71	0.53	0.14	0.09	0.1100	51.25	(180)
GSC 01387-00475	A	0.2178	–	0.474	–	50	1.32	76	6690	6524	0.44	0.21	0.66	0.50	0.19	0.09	0.1838	51.10	(181)

REFERENCES

Adalalı S., Soydugan E., 2024, New Astron., 112, 102270

Albayrak B., Djurašević G., Selam S. O., Atanacković-Vukmanović O., Yılmaz M., 2005, New Astron., 10, 163

Alton K. B., Nelson R. H., 2018, MNRAS, 479, 3197

Alton K. B., Nelson R. H., Boyd D. R. S., 2018a, Acta Astron., 68, 159

Alton K. B., Nelson R. H., Terrell D., 2018b, Information Bulletin on Variable Stars, 6256, 1

Alvarez G. E., Sowell J. R., Williamon R. M., Lapasset E., 2015, PASP, 127, 742

Applegate J. H., 1992, ApJ, 385, 621

Arbutina B., 2007, MNRAS, 377, 1635

Arbutina B., 2009, MNRAS, 394, 501

Baran A., Zola S., Rucinski S. M., Kreiner J. M., Siwak M., Drozdz M., 2004, Acta Astron., 54, 195

Barden S. C., 1985, ApJ, 295, 162

Barden R. E., Logan E. R., Branthaver J. F., Neet K. E., 1984, Organic Geochemistry, 5, 217

Barnes J. R., Lister T. A., Hilditch R. W., Collier Cameron A., 2004, MNRAS, 348, 1321

Barone F., di Fiore L., Milano L., Russo G., 1993, ApJ, 407, 237

Bell S. A., Malcolm G. J., 1987, MNRAS, 226, 899

Bellm E. C., et al., 2019, PASP, 131, 018002

Binnendijk L., 1970, Vistas in Astronomy, 12, 217

Butters O. W., et al., 2010, A&A, 520, L10

Caballero-García M. D., Torres G., Ribas I., Rísquez D., Montesinos B., Mas-Hesse J. M., Domingo A., 2010, A&A, 514, A36

Cabrera N. E., Sowell J. R., Williamon R. M., Collins T. F., Fekel F. C., Williamson M. H., Muterspaugh M. W., 2014, PASP, 126, 121

Cheng Y., Zhang L.-y., Han X. L., Long L., Lu H., Yue Q., Jiang L., 2019, AJ, 158, 193

Chochol D., van Houten C. J., Pribulla T., Grygar J., 2001, Contributions of the Astronomical Observatory Skalnate Pleso, 31, 5

Christopoulou P. E., Papageorgiou A., 2013, AJ, 146, 157

Christopoulou P. E., Parageorgiou A., Chrysopoulos I., 2011, AJ, 142, 99

Christopoulou P.-E., Lalounta E., Papageorgiou A., Ferreira Lopes C. E., Catelan M., Drake A. J., 2022, MNRAS, 512, 1244

Csák B., Kiss L. L., Vinkó J., Alfaro E. J., 2000, A&A, 356, 603

Cseki A., 2013, Serbian Astronomical Journal, 186, 47

Cui X.-Q., et al., 2012, Research in Astronomy and Astrophysics, 12, 1197

D 2006, LPI Bulletin, 107, 13

Davis P. J., Siess L., Deschamps R., 2014, A&A, 570, A25

Deb S., Singh H. P., 2011, MNRAS, 412, 1787

Devarapalli S. P., Jagirdar R., Prasad R. M., Thomas V. S., Ahmed S. A., Gralapally R., Das J. P., 2020, MNRAS, 493, 1565

Djurašević G., Rovithis-Livaniou H., Rovithis P., Erkapić S., Milovanović N., 2001, A&A, 367, 840

Djurašević G., Yılmaz M., Baştürk Ö., Kılıçoğlu T., Latković O., Çalışkan Ş., 2011, A&A, 525, A66

Djurašević G., et al., 2013, AJ, 145, 80

Drechsel H., Rahe J., Wargau W., Wolf B., 1982, A&A, 110, 246

Du B., et al., 2016, ApJS, 227, 27

Duerbeck H. W., Rucinski S. M., 2007, AJ, 133, 169

Eastman J., Siverd R., Gaudi B. S., 2010, PASP, 122, 935

Eggleton P. P., 2012, Journal of Astronomy and Space Sciences, 29, 145

Eker Z., Demircan O., Bilir S., Karataş Y., 2006, MNRAS, 373, 1483

Eker Z., Demircan O., Bilir S., 2008a, MNRAS, 386, 1756

Eker Z., et al., 2008b, MNRAS, 389, 1722

Ekmekçi F., et al., 2012, New Astron., 17, 603

Er-gang Z., Sheng-bang Q., Soonthornthum B., Poshyachinda S., Xiao Z., Sarotsakulchai T., Jia Z., Wen-ping L., 2019, ApJ, 871, L10

Erdem A., Özkardeş B., 2006, New Astron., 12, 192

Erdem A., Özkardeş B., 2009, New Astron., 14, 321

Erkan N., Ulaş B., 2016, New Astron., 46, 73

Flannery B. P., 1976, ApJ, 205, 217

Gaia Collaboration et al., 2016, A&A, 595, A1

Gaia Collaboration et al., 2023, A&A, 674, A1

References. (1)Zhao et al. (2014), (2)Stickland et al. (1994), (3)Yaşarsoy & Yakut (2013), (4)Rucinski (1992), (5)Drechsel et al. (1982), (6)Li et al. (2022b), (7)Terrell et al. (2003), (8)Wang et al. (2025), (9)Djurašević et al. (2013), (10)Pribulla et al. (2011), (11)Cabrera et al. (2014), (12)Rucinski et al. (2003), (13)Gazeas et al. (2006), (14)Zhou et al. (2016a), (15)Duerbeck & Rucinski (2007), (16)Sarotsakulchai et al. (2018), (17)Rucinski et al. (2002), (18)Rodríguez et al. (1998), (19)Yakut et al. (2004), (20)Yakut & Eggleton (2005), (21)Alvarez et al. (2015), (22)Çiçek (2011), (23)Pribulla et al. (2006), (24)Tian et al. (2018), (25)Yang et al. (2019), (26)Bell & Malcolm (1987), (27)Siwak et al. (2010), (28)Li & Qian (2013b), (29)Zola et al. (2005), (30)Csák et al. (2000), (31)Pribulla et al. (2002), (32)Rucinski et al. (2001), (33)Yuan (2011), (34)Rucinski et al. (2005), (35)Zhu et al. (2005), (36)Zhou et al. (2015), (37)Rucinski et al. (2008), (38)Lee & Park (2018), (39)Lee et al. (2014), (40)Deb & Singh (2011), (41)Özkardeş & Erdem (2012), (42)Partovi et al. (2021), (43)Zola et al. (2004), (44)Yang et al. (2005), (45)Pych et al. (2011), (46)Pribulla et al. (2009b), (47)Çalışkan et al. (2014), (48)Papageorgiou & Christopoulou (2015), (49)Hilditch & King (1986), (50)Chochol et al. (2001), (51)Albayrak et al. (2005), (52)Kreiner et al. (2003), (53)Goecking & Duerbeck (1993), (54)Wolf et al. (2000), (55)Park et al. (2013), (56)Ekmekçi et al. (2012), (57)Christopoulou et al. (2022), (58)Zola et al. (2012), (59)Li et al. (2016a), (60)Baran et al. (2004), (61)Gazeas et al. (2005), (62)Papageorgiou et al. (2015), (63)Wadhwa & Zealey (2004), (64)Devarapalli et al. (2020), (65)Erkan & Ulaş (2016), (66)Lee et al. (2015), (67)Lee et al. (2011), (68)Yildirim et al. (2019), (69)Molnar et al. (2017), (70)Özkardeş et al. (2009), (71)Xiao et al. (2016), (72)Yang et al. (2004), (73)Oh et al. (2010), (74)Şenavcı et al. (2008), (75)Qian et al. (2005), (76)Selam et al. (2018), (77)Zhou et al. (2016b), (78)Şenavcı et al. (2016), (79)Ulaş & Ulusoy (2014), (80)Pych et al. (2004), (81)Gomez-Forrellad et al. (1999), (82)Gazeas & Niarchos (2005), (83)Pribulla et al. (2009a), (84)Tas & Evren (2006), (85)Hambálek & Pribulla (2017), (86)Yang (2012), (87)Goecking et al. (1994), (88)Kim et al. (2003), (89)Caballero-García et al. (2010), (90)Özdemir et al. (2002), (91)Gürol et al. (2011b), (92)Erdem & Özkardeş (2009), (93)Liu et al. (1996), (94)Yamasaki et al. (1988), (95)Yang & Liu (2003), (96)D (2006), (97)Gürol (2016), (98)Djurašević et al. (2011), (99)Kjurkchieva et al. (2019c), (100)Kjurkchieva et al. (2018a), (101)Zola et al. (2010), (102)Zasche & Uhlář (2010), (103)Lu & Rucinski (1993), (104)Liu et al. (2009), (105)Liu et al. (2019), (106)Xia et al. (2025), (107)Szalai et al. (2007), (108)Alton & Nelson (2018), (109)Christopoulou & Papageorgiou (2013), (110)Gürol et al. (2011a), (111)Alton et al. (2018b), (112)Nelson et al. (2014), (113)Gürol et al. (2015a), (114)Oh et al. (2007), (115)Nelson & Robb (2015), (116)Pi et al. (2017), (117)Selam et al. (2005), (118)Kjurkchieva et al. (2018c), (119)Zheng et al. (2021), (120)Kjurkchieva et al. (2019b), (121)Yılmaz et al. (2015), (122)Djurašević et al. (2001), (123)Li & Qian (2013a), (124)Barone et al. (1993), (125)Leung (1976), (126)Lu et al. (2007), (127)Luo et al. (2017), (128)Yang et al. (2013), (129)Gorda (2016), (130)Barnes et al. (2004), (131)He et al. (2009), (132)Kamalifar et al. (2020), (133)Liao et al. (2019), (134)Erdem & Özkardeş (2006), (135)Cseki (2013), (136)Li et al. (2015b), (137)Nelson (2010), (138)Kaluzny & Rucinski (1986), (139)Kjurkchieva et al. (2018b), (140)Li et al. (2016b), (141)Lapasset & Gomez (1990), (142)Xiang et al. (2015), (143)Maceroni et al. (1984), (144)Liu et al. (2011), (145)Hasanzadeh et al. (2015), (146)Nelson & Alton (2019), (147)Linnell (1991), (148)Li et al. (2014), (149)Kjurkchieva et al. (2018d), (150)Yang & Liu (1999), (151)Gürol et al. (2015c), (152)Gürol et al. (2015b), (153)Guo et al. (2020), (154)Ostadnezhad et al. (2014), (155)Zhu et al. (2013), (156)Liu et al. (2012), (157)Vanko et al. (2001), (158)Alton et al. (2018a), (159)Christopoulou et al. (2011), (160)Kopacki & Pigulski (1995), (161)Qian (2001), (162)Sarotsakulchai et al. (2019), (163)Gürol et al. (2016), (164)Li et al. (2015a), (165)Mitnyan et al. (2018), (166)Gazeas et al. (2021), (167)Yang et al. (2009), (168)Kjurkchieva et al. (2019a), (169)Hill et al. (1989), (170)Lu et al. (2001), (171)Kriwattanawong & Poojon (2013), (172)Zhang & Qian

(2020), (173)Hrivnak et al. (1995), (174)Yue et al. (2019), (175)Lohr et al. (2014), (176)Michel & Kjurkchieva (2019), (177)Samec et al. (2004), (178)Zhang & Zhang (2004), (179)Lohr et al. (2015), (180)Köse et al. (2011), (181)Yang et al. (2010).
Gao X.-Y., Cai Y.-W., Li K., Gao A., Shao Y.-D., 2022, New Astron., 95, 101800
Gazeas K., Niarchos P., 2005, Aerospace Research in Bulgaria, 20, 193
Gazeas K. D., et al., 2005, Acta Astron., 55, 123
Gazeas K. D., Niarchos P. G., Zola S., Kreiner J. M., Rucinski S. M., 2006, Acta Astron., 56, 127
Gazeas K., et al., 2021, MNRAS, 501, 2897
Goecking K. D., Duerbeck H. W., 1993, A&A, 278, 463
Goecking K. D., Duerbeck H. W., Plewa T., Kaluzny J., Schertl D., Weigelt G., Flin P., 1994, A&A, 289, 827
Gomez-Forrellad J. M., Garcia-Melendo E., Guarro-Flo J., Nomen-Torres J., Vidal-Sainz J., 1999, Information Bulletin on Variable Stars, 4702, 1
Gorda S. Y., 2016, Astrophysical Bulletin, 71, 64
Guo D.-F., Li K., Gao X., Gao D.-Y., Xu Z.-J., Sun G.-Y., Liu F., Zhang C.-M., 2020, MNRAS, 497, 3381
Guo D.-F., et al., 2022, MNRAS, 517, 1928
Gürol B., 2016, New Astron., 47, 57
Gürol B., et al., 2011a, New Astron., 16, 242
Gürol B., Terzioğlu Z., Gürsoytrak S. H., Gökay G., Derman E., 2011b, Astronomische Nachrichten, 332, 690
Gürol B., Bradstreet D. H., Okan A., 2015a, New Astron., 36, 100
Gürol B., Gürsoytrak S. H., Bradstreet D. H., 2015b, New Astron., 39, 9
Gürol B., Bradstreet D. H., Demircan Y., Gürsoytrak S. H., 2015c, New Astron., 41, 26
Gürol B., Gökay G., Saral G., Gürsoytrak S. H., Cerit S., Terzioğlu Z., 2016, New Astron., 46, 31
Hambálek L., Pribulla T., 2017, in Balega Y. Y., Kudryavtsev D. O., Romanyuk I. I., Yakunin I. A., eds, Astronomical Society of the Pacific Conference Series Vol. 510, Stars: From Collapse to Collapse. p. 372
Hasanzadeh A., Farsian F., Nemati M., 2015, New Astron., 34, 262
He J. J., Qian S. B., Fernández Lajús E., Fariña C., 2009, AJ, 138, 1465
Hilditch R. W., King D. J., 1986, MNRAS, 223, 581
Hill G., Fisher W. A., Holmgren D., 1989, A&A, 211, 81
Hrivnak B. J., Guinan E. F., Lu W., 1995, ApJ, 455, 300
Huang S.-S., 1966, Annales d'Astrophysique, 29, 331
Hurley J. R., Tout C. A., Pols O. R., 2002, MNRAS, 329, 897
Hut P., 1980, A&A, 92, 167
Jayasinghe T., et al., 2019, MNRAS, 486, 1907
Kaluzny J., Rucinski S. M., 1986, AJ, 92, 666
Kamalifar Z., Abedi A., Roobiat K. Y., 2020, New Astron., 78, 101354
Kim C.-H., Lee J. W., Kim H.-I., Kyung J.-M., Koch R. H., 2003, AJ, 126, 1555
Kim C.-H., Jeong J. H., Lee Y. S., 2006, Journal of Astronomy and Space Sciences, 23, 105
Kjurkchieva D. P., Popov V. A., Lyubenova Vasileva D., Petrov N. I., 2018a, Research in Astronomy and Astrophysics, 18, 046
Kjurkchieva D. P., Popov V. A., Vasileva D. L., Petrov N. I., 2018b, New Astron., 62, 46
Kjurkchieva D. P., Popov V. A., Petrov N. I., 2018c, AJ, 156, 77
Kjurkchieva D. P., Marchev D. V., Popov V. A., 2018d, Astronomische Nachrichten, 339, 472
Kjurkchieva D. P., Popov V. A., Petrov N. I., 2019a, New Astron., 68, 20
Kjurkchieva D., Stateva I., Popov V. A., Marchev D., 2019b, AJ, 157, 73
Kjurkchieva D. P., Popov V. A., Petrov N. I., 2019c, AJ, 158, 186
Knote M. F., Caballero-Nieves S. M., Gokhale V., Johnston K. B., Perlman E. S., 2022, ApJS, 262, 10
Kobulnicky H. A., Molnar L. A., Cook E. M., Henderson L. E., 2022, ApJS, 262, 12
Kochanek C. S., et al., 2017, PASP, 129, 104502
Kopacki G., Pigulski A., 1995, Acta Astron., 45, 753
Köse O., Kalomeni B., Keskin V., Ulaş B., Yakut K., 2011, Astronomische Nachrichten, 332, 626
Kraft R. P., 1967, Publications of the Astronomical Society of the Pacific, 79, 395
Kreiner J. M., et al., 2003, A&A, 412, 465
Kriwattanawong W., Poojon P., 2013, Research in Astronomy and Astrophysics, 13, 1330
Kudak V., Fedurco M., Perig V., Parimucha Š., 2021, Research in Astronomy and Astrophysics, 21, 174
Kuiper G. P., 1941, ApJ, 93, 133
Kwee K. K., van Woerden H., 1956, Bull. Astron. Inst. Netherlands, 12, 327
Landin N. R., Mendes L. T. S., Vaz L. P. R., 2009, A&A, 494, 209
Lapasset E., Gomez M., 1990, A&A, 231, 365
Lee J. W., Park J.-H., 2018, PASP, 130, 034201
Lee J. W., Lee C.-U., Kim S.-L., Kim H.-I., Park J.-H., 2011, PASP, 123, 34
Lee J. W., Park J.-H., Hong K., Kim S.-L., Lee C.-U., 2014, AJ, 147, 91
Lee J. W., Youn J.-H., Park J.-H., Wolf M., 2015, AJ, 149, 194
Leung K. C., 1976, PASP, 88, 936
Li C., Hong J., 2018, MNRAS, 476, 5274
Li K., Qian S. B., 2013a, New Astron., 21, 46
Li K., Qian S. B., 2013b, New Astron., 22, 57
Li L., Zhang F., Han Z., Jiang D., 2007, ApJ, 662, 596
Li K., Hu S. M., Jiang Y. G., Chen X., Ren D. Y., 2014, New Astron., 30, 64
Li K., Hu S., Guo D., Jiang Y., Gao D., Chen X., 2015a, New Astron., 41, 17
Li K., Hu S. M., Guo D. F., Jiang Y. G., Gao Y. G., Chen X., Odell A. P., 2015b, AJ, 149, 120
Li H.-L., Wei J.-Y., Yang Y.-G., Dai H.-F., 2016a, Research in Astronomy and Astrophysics, 16, 2
Li K., Gao D. Y., Hu S. M., Guo D. F., Jiang Y. G., Chen X., 2016b, Ap&SS, 361, 63
Li K., Xia Q. Q., Hu S. M., Guo D. F., Chen X., 2018, PASP, 130, 074201
Li K., et al., 2019a, Research in Astronomy and Astrophysics, 19, 147
Li K., Xia Q.-Q., Michel R., Hu S.-M., Guo D.-F., Gao X., Chen X., Gao D.-Y., 2019b, MNRAS, 485, 4588
Li K., Kim C.-H., Xia Q.-Q., Michel R., Hu S.-M., Gao X., Guo D.-F., Chen X., 2020, AJ, 159, 189
Li K., et al., 2021, AJ, 162, 13
Li K., Gao X., Liu X.-Y., Gao X., Li L.-Z., Chen X., Sun G.-Y., 2022a, AJ, 164, 202
Li F. X., Liao W. P., Qian S. B., Fernández Lajús E., Zhang J., Zhao E. G., 2022b, ApJ, 924, 30
Li K., et al., 2024, A&A, 692, L4
Li L.-Z., et al., 2025, MNRAS, 537, 2258
Liao W.-P., Qian S.-B., Soonthornthum B., Sarotsakulchai T., Zhu L.-Y., Zhang J., Irina V., 2017, PASP, 129, 124204
Liao W. P., Qian S. B., Sarotsakulchai T., 2019, AJ, 157, 207
Linnell A. P., 1991, ApJ, 374, 307
Liu Q.-Y., Yang Y.-L., 2003, Chinese J. Astron. Astrophys., 3, 142
Liu Q., Soonthornthum B., Yang Y., Gu S., Niparugs S., Aniwat Sooksawat M. L., Wang B., Naksata M., 1996, A&AS, 118, 453
Liu L., Qian S. B., He J. J., Zhang J., Li L. J., 2009, Ap&SS, 321, 19
Liu L., Qian S. B., Zhu L. Y., He J. J., Li L. J., 2011, AJ, 141, 147
Liu L., Qian S.-B., He J.-J., Liao W.-P., Zhu L.-Y., Zhao E., 2012, PASJ, 64, 48
Liu J., et al., 2019, PASP, 131, 084202
Liu X.-Y., et al., 2023, MNRAS, 519, 5760
Liu F., et al., 2024, MNRAS, 527, 6406
Lohr M. E., Hodgkin S. T., Norton A. J., Kolb U. C., 2014, A&A, 563, A34
Lohr M. E., et al., 2015, A&A, 578, A103
Long L., Zhang L.-Y., Han X. L., Lu H.-P., Pi Q.-f., Yue Q., 2019, MNRAS, 487, 5520
Lu W. X., Rucinski S. M., 1993, AJ, 106, 361
Lu W., Rucinski S. M., Ogłoza W., 2001, AJ, 122, 402
Lu W., Hrivnak B. J., Rush B. W., 2007, AJ, 133, 255
Lucy L. B., 1967a, Z. Astrophys., 65, 89
Lucy L. B., 1967b, AJ, 72, 813
Lucy L. B., 1968, ApJ, 151, 1123
Lucy L. B., 1976, ApJ, 205, 208
Luo X., Wang K., Zhang X., Deng L., Luo Y., Luo C., 2017, AJ, 154, 99
Maceroni C., Milano L., Russo G., 1984, A&AS, 58, 405
Masci F. J., et al., 2019, PASP, 131, 018003

Matekov A., Meng F., Qian S., Asfandiyarov I., Li L., Ehgamberdiev S., Zhu L., 2023, PASJ, 75, 701
Michel R., Kjurkchieva D., 2019, New Astron., 68, 51
Mitnyan T., et al., 2018, A&A, 612, A91
Molnar L. A., et al., 2017, ApJ, 840, 1
Molnar L. A., Blain M. G., Cook E. M., Whitten S. M., Kobulnicky H., 2019, in American Astronomical Society Meeting Abstracts #233. p. 448.05
Molnar L., Avery A., Blain M., Henderson L., Lau J. F., Le G. M., 2022, in American Astronomical Society Meeting #240. p. 308.01
Montes D., de Castro E., Fernandez-Figueroa M. J., Cornide M., 1995, A&AS, 114, 287
Nelson R. H., 2010, Information Bulletin on Variable Stars, 5951, 1
Nelson R. H., Alton K. B., 2019, Information Bulletin on Variable Stars, 6266
Nelson R. H., Robb R. M., 2015, Information Bulletin on Variable Stars, 6134, 1
Nelson R. H., Şenavci H. V., Baştürk Ö., Bahar E., 2014, New Astron., 29, 57
O'Connell D. J. K., 1951, Publications of the Riverview College Observatory, 2, 85
Oh K. D., Kim C. H., Kim H. I., Lee W. B., 2007, in Kang Y. W., Lee H. W., Leung K. C., Cheng K. S., eds, Astronomical Society of the Pacific Conference Series Vol. 362, The Seventh Pacific Rim Conference on Stellar Astrophysics. p. 82
Oh K.-D., Kim H.-I., Sung E.-C., 2010, Journal of Astronomy and Space Sciences, 27, 69
Ostadnezhad S., Delband M., Hasanzadeh A., 2014, New Astron., 31, 14
Özdemir S., Demircan O., Erdem A., Çiçek C., Bulut İ., Soydugan E., Soydugan F., 2002, A&A, 387, 240
Özkardeş B., Erdem A., 2012, New Astron., 17, 143
Özkardeş B., Erdem A., Bakış V., 2009, New Astron., 14, 461
Papageorgiou A., Christopoulou P. E., 2015, AJ, 149, 168
Papageorgiou A., Christopoulou P. E., Pribulla T., Vaňko M., 2015, Ap&SS, 357, 59
Park J.-H., Lee J. W., Kim S.-L., Lee C.-U., Jeon Y.-B., 2013, PASJ, 65, 1
Partovi M., Abedi A., Roobiat K. Y., 2021, Serbian Astronomical Journal, 203, 29
Pavlenko Y. V., Evans A., Banerjee D. P. K., Southworth J., Shahbandeh M., Davis S., 2018, A&A, 615, A120
Pecaut M. J., Mamajek E. E., 2013, ApJS, 208, 9
Pi Q.-f., Zhang L.-y., Bi S.-l., Han X. L., Wang D.-m., Lu H.-p., 2017, AJ, 154, 260
Pi Q.-f., Zhang L.-y., Bi S.-l., Han X. L., Lu H.-p., Yue Q., Long L., Yan Y., 2019, ApJ, 877, 75
Poro A., et al., 2024a, Research in Astronomy and Astrophysics, 24, 015002
Poro A., et al., 2024b, New Astron., 110, 102227
Poro A., Tanriver M., Michel R., Paki E., 2024c, PASP, 136, 024201
Pribulla T., Chochol D., Vanko M., Parimucha S., 2002, Information Bulletin on Variable Stars, 5258, 1
Pribulla T., Kreiner J. M., Tremko J., 2003a, VizieR Online Data Catalog: Catalogue of field contact binary stars (Pribulla+, 2003), VizieR On-line Data Catalog: V/119. Originally published in: 2003CoSka..33...38P
Pribulla T., Chochol D., Vittone A. A., 2003b, Chinese Journal of Astronomy and Astrophysics Supplement, 3, 361
Pribulla T., Kreiner J. M., Tremko J., 2003c, Contributions of the Astronomical Observatory Skalnate Pleso, 33, 38
Pribulla T., et al., 2006, AJ, 132, 769
Pribulla T., et al., 2009a, AJ, 137, 3646
Pribulla T., et al., 2009b, AJ, 137, 3655
Pribulla T., Vaňko M., Chochol D., Hambálek Ľ., Parimucha Š., 2011, Astronomische Nachrichten, 332, 607
Pych W., et al., 2004, AJ, 127, 1712
Pych W., et al., 2011, AJ, 141, 207
Qian S., 2001, MNRAS, 328, 635
Qian S., 2003, MNRAS, 342, 1260
Qian S. B., Yang Y. G., Soonthornthum B., Zhu L. Y., He J. J., Yuan J. Z., 2005, AJ, 130, 224
Qian S. B., Yuan J. Z., Xiang F. Y., Soonthornthum B., Zhu L. Y., He J. J., 2007, AJ, 134, 1769
Qian S. B., et al., 2015, ApJ, 798, L42
Rasio F. A., 1995, ApJ, 444, L41
Ricker G. R., et al., 2015, Journal of Astronomical Telescopes, Instruments, and Systems, 1, 014003
Robertson J. A., Eggleton P. P., 1977, MNRAS, 179, 359
Rodríguez E., et al., 1998, A&A, 336, 920
Ruciński S. M., 1969, Acta Astron., 19, 245
Rucinski S. M., 1992, AJ, 103, 960
Rucinski S. M., 2001, AJ, 122, 1007
Rucinski S. M., 2006, MNRAS, 368, 1319
Rucinski S. M., Lu W., Mochnacki S. W., Ogłoza W., Stachowski G., 2001, AJ, 122, 1974
Rucinski S. M., Lu W., Capobianco C. C., Mochnacki S. W., Blake R. M., Thomson J. R., Ogłoza W., Stachowski G., 2002, AJ, 124, 1738
Rucinski S. M., et al., 2003, AJ, 125, 3258
Rucinski S. M., et al., 2005, AJ, 130, 767
Rucinski S. M., et al., 2008, AJ, 136, 586
Samec R. G., Faulkner D. R., Williams D. B., 2004, AJ, 128, 2997
Sarotsakulchai T., et al., 2018, AJ, 156, 199
Sarotsakulchai T., et al., 2019, PASJ, 71, 34
Selam S., Albayrak B., Yilmaz M., Şenavci H. V., Özavci İ., Çetintaş C., 2005, Ap&SS, 296, 305
Selam S. O., Esmer E. M., Şenavcı H. V., Bahar E., Yörükoğlu O., Yılmaz M., Baştürk Ö., 2018, Ap&SS, 363, 34
Shappee B. J., et al., 2014, ApJ, 788, 48
Shaw J., 1994, Memorie della Società Astronomia Italiana, Vol. 65, p. 95, 65, 95
Shi A., et al., 2025, ApJS, 280, 26
Siwak M., Zola S., Koziel-Wierzbowska D., 2010, Acta Astron., 60, 305
Stickland D. J., Koch R. H., Pachoulakis I., Pfeiffer R. J., 1994, The Observatory, 114, 107
Strassmeier K. G., 2009, A&ARv, 17, 251
Szalai T., Kiss L. L., Mészáros S., Vinkó J., Csizmadia S., 2007, A&A, 465, 943
Tas G., Evren S., 2006, Information Bulletin on Variable Stars, 5687, 1
Terrell D., Wilson R. E., 2005, Ap&SS, 296, 221
Terrell D., Munari U., Zwitter T., Nelson R. H., 2003, AJ, 126, 2988
Tian X.-M., Zhu L.-Y., Qian S.-B., Li L.-J., Jiang L.-Q., 2018, Research in Astronomy and Astrophysics, 18, 020
Ulaş B., Ulusoy C., 2014, New Astron., 31, 56
Van Hamme W., 1993, AJ, 106, 2096
Vanko M., Pribulla T., Chochol D., Parimucha S., Kim C. H., Lee J. W., Han J. Y., 2001, Contributions of the Astronomical Observatory Skalnate Pleso, 31, 129
Völschow M., Schleicher D. R. G., Perdelwitz V., Banerjee R., 2016, A&A, 587, A34
Wadhwa S. S., Zealey W. J., 2004, Ap&SS, 291, 21
Wang S.-G., Su D.-Q., Chu Y.-Q., Cui X., Wang Y.-N., 1996, Appl. Opt., 35, 5155
Wang J.-Y., et al., 2025, ApJ, 979, 69
Williams P. S., Roxburgh I. W., 1976, MNRAS, 176, 81
Wilsey N. J., Beaky M. M., 2009, Society for Astronomical Sciences Annual Symposium, 28, 107
Wilson O. C., 1978, ApJ, 226, 379
Wilson R. E., 1979, ApJ, 234, 1054
Wilson R. E., 1994, PASP, 106, 921
Wilson R. E., Devinney E. J., 1971, ApJ, 166, 605
Wolf M., Molík P., Hornoch K., Šarounová L., 2000, A&AS, 147, 243
Xia Q., et al., 2025, AJ, 169, 139
Xiang F.-Y., Yu Y.-X., Xiao T.-Y., 2015, AJ, 149, 62
Xiao Z., Shengbang Q., Binghe H., Hao L., Jia Z., 2016, PASJ, 68, 102
Yaşarsoy B., Yakut K., 2013, AJ, 145, 9
Yakut K., Eggleton P. P., 2005, ApJ, 629, 1055
Yakut K., Kalomeni B., İbanoğlu C., 2004, A&A, 417, 725
Yamasaki A., Jugaku J., Seki M., 1988, AJ, 95, 894
Yang Y.-G., 2012, Research in Astronomy and Astrophysics, 12, 419
Yang Y., Liu Q., 1999, A&AS, 136, 139
Yang Y., Liu Q., 2003, AJ, 126, 1960
Yang Y.-G., Qian S.-B., 2015, AJ, 150, 69

Yang Y. G., Qian S. B., Zhu C. H., 2004, PASP, 116, 826
Yang Y.-G., Qian S.-B., Zhu L.-Y., He J.-J., Yuan J.-Z., 2005, PASJ, 57, 983
Yang Y. G., Qian S. B., Zhu L. Y., He J. J., 2009, AJ, 138, 540
Yang Y. G., Wei J. Y., Li H. L., 2010, New Astron., 15, 155
Yang Y. G., Qian S. B., Zhang L. Y., Dai H. F., Soonthornthum B., 2013, AJ, 146, 35
Yang Y., Yuan H., Dai H., 2019, AJ, 157, 111
Yildirim M. F., Aliçavuş F., Soydugan F., 2019, Research in Astronomy and Astrophysics, 19, 010
Yıldız M., 2014, MNRAS, 437, 185
Yildiz M., Doğan T., 2013, MNRAS, 430, 2029
Yılmaz M., Baştürk Ö., Özavcı İ., Şenavcı H. V., Selam S. O., 2015, New Astron., 34, 271
Yuan J.-Z., 2011, Research in Astronomy and Astrophysics, 11, 1158
Yue Q., Zhang L.-Y., Han X.-M. L., Lu H.-P., Long L., Yan Y., 2019, Research in Astronomy and Astrophysics, 19, 097
Zasche P., Uhlář R., 2010, A&A, 519, A78
Zervas K., Christopoulou P.-E., Papageorgiou A., 2024, ApJ, 961, 97
Zhang X.-D., Qian S.-B., 2020, MNRAS, 497, 3493
Zhang X. B., Zhang R. X., 2004, MNRAS, 347, 307
Zhang B., et al., 2021, ApJS, 256, 14
Zhang X., Chen X., Fu J., Li Y., 2023, MNRAS, 523, 1394
Zhang B., Gao Y.-D., Li K., Wang J.-J., Zhang X.-D., Xiao W.-J., 2025, MNRAS, 537, 3366
Zhao G., Zhao Y.-H., Chu Y.-Q., Jing Y.-P., Deng L.-C., 2012, Research in Astronomy and Astrophysics, 12, 723
Zhao E., Qian S., Li L., He J., Liu L., Wang J., Zhang J., 2014, New Astron., 26, 112
Zheng S.-Y., Li K., Xia Q.-Q., 2021, MNRAS, 506, 4251
Zhou D.-Q., Leung K.-C., 1990, ApJ, 355, 271
Zhou X., Qian S., He J., Zhang J., Jiag L., 2015, PASJ, 67, 98
Zhou X., Qian S. B., Zhang J., Zhang B., Kreiner J., 2016a, AJ, 151, 67
Zhou X., Qian S. B., Zhang J., Jiang L. Q., Zhang B., Kreiner J., 2016b, ApJ, 817, 133
Zhu L. Y., Qian S. B., Soonthornthum B., Yang Y. G., 2005, AJ, 129, 2806
Zhu L. Y., Qian S. B., Soonthornthum B., He J. J., Liu L., 2011, AJ, 142, 124
Zhu L. Y., Qian S. B., Liu N. P., Liu L., Jiang L. Q., 2013, AJ, 145, 39
Zola S., et al., 2004, Acta Astron., 54, 299
Zola S., et al., 2005, Acta Astron., 55, 389
Zola S., Gazeas K., Kreiner J. M., Ogloza W., Siwak M., Koziel-Wierzbowska D., Winiarski M., 2010, MNRAS, 408, 464
Zola S., Nelson R. H., Şenavcı H. V., Szymanski T., Kuźmicz A., Winiarski M., Jableka D., 2012, New Astron., 17, 673
Zola S., Baran A., Debski B., Jableka D., 2017, MNRAS, 466, 2488
Zwitter T., Munari U., Marrese P. M., Prša A., Milone E. F., Boschi F., Tomov T., Siviero A., 2003, A&A, 404, 333
Çalışkan Ş., et al., 2014, AJ, 148, 126
Çiçek C., 2011, New Astron., 16, 12
Şenavcı H. V., Nelson R. H., Özavcı İ., Selam S. O., Albayrak B., 2008, New Astron., 13, 468
Şenavcı H. V., Doğruel M. B., Nelson R. H., Yılmaz M., Selam S. O., 2016, Publ. Astron. Soc. Australia, 33, e043

This paper has been typeset from a TEX/LATEX file prepared by the author.